

MECHANICAL INTEGRITY OF CYLINDRICAL 21700 LITHIUM-ION
BATTERIES BASED ON ELECTROCHEMICAL STATUS

by

Aditya Nitin Sonwane

A thesis submitted to the faculty of
The University of North Carolina at Charlotte
in partial fulfillment of the requirements
for the degree of Master of Science in
Mechanical Engineering

Charlotte

2020

Approved by:

Dr. Jun Xu

Dr. Mesbah Uddin

Dr. Amirhossein Ghasemi

ABSTRACT

ADITYA NITIN SONWANE. Mechanical Integrity of cylindrical 21700 lithium-ion batteries based on electrochemical status. (Under the direction of DR. JUN XU)

The sustainability requirement for both the energy and environment has triggered clean energy usage in the automotive industry such that electric vehicles (EVs) powered by lithium-ion batteries (LIBs) have now become the popular choices for current internal combustion automobiles. However, one of the biggest hurdles that discourage customers from purchasing EVs is the safety issues of LIBs. The situation even deteriorates with the recent application of higher energy density LIBs in vehicles for longer ranges. One of the direct causations of the internal short circuit and thermal runaway issues are possible crash accidents. To tackle this problem, in this work, the mechanical behaviors of the widely used 21700 LIB cells and the electrodes are targeted. Systematic characterizations considering strain rate effects, material directions, state of charges (SOCs), and charging cycles are conducted for anodes, cathodes, and the current collectors. Both anodes and cathodes are strongly strain rate dependent. Particularly, SOC has a significant influence over the mechanical behaviors of the anode due to the intercalation induced particle expansion. In the meantime, several finite element models for anodes and cathodes are developed for future full cell modeling. A strong electrochemical effect over mechanical behaviors is observed and discovered. Results provide a basic and comprehensive understanding of the mechanical behaviors of the electrodes used in the 21700 NCM batteries and lay a strong foundation for future multiphysics modeling from the cell level, pack level, and up to the EV level.

DEDICATION

Dedicated to my loving parents Nitin and Kalpana whose unconditional love and support thrived me to reach for heights I could have never imagined. I would also like to dedicate my work to my beloved sister Aishwarya, my grandfather Devidasrao and my late grandmother Chandralekha whose guidance has helped me throughout.

To my friends and my teachers for their word of advice, encouragement and inspiration all the way.

ACKNOWLEDGEMENTS

I would like to express my deep and sincere gratitude to my thesis advisor, Dr. Jun Xu, for offering a learning opportunity to explore the research in batteries with his invaluable guidance, motivation, and empathy towards my fellow graduate students and me. I am grateful for the time and commitment Dr. Xu has put towards training and facilitating me throughout my thesis. I would like to extend my gratitude towards my committee members Dr. Mesbah Uddin and Dr. Amirhossein Ghasemi, for their time and valuable feedback. I also very much appreciate Dr. Youxing Chen for his support and guidance for using the SEM imaging machine.

I would like to thank my lab members and Ph.D. students, Mr. Chunhao Yuan, Mr. Xiang Gao, Ms. Wen Zhang, and Mr. Yikai Jai, for guiding and advising me with their technical knowledge. I would like to thank Ms. Liuquig Yang for her time and commitment to help me work on SEM imaging machine. I would also like to thank my friends Mr. Parth Amrapurkar, Mr. Shreyas Tuljapurkar, and Ms. Sheetal Patil, for their consistent support throughout. Ultimately, I would like to express my appreciation to The University of North Carolina at Charlotte and Motorsports Research facility and faculty for the research opportunity aiding in the completion of my thesis.

TABLE OF CONTENTS

LIST OF TABLES	viii
LIST OF FIGURES	ix
LIST OF ABBREVIATIONS	xiv
CHAPTER 1: INTRODUCTION	1
1.1 Background.....	1
1.2 Literature review.....	2
1.3 Objective.....	9
CHAPTER 2: EXPERIMENTAL METHODOLOGY	11
2.1 Cycling methodology and procedure for experiment	11
2.2 Tensile testing procedure	15
CHAPTER 3: SIMULATION METHODOLOGY	21
3.1 Material properties and simulation module	21
3.2 Governing equations and model setup	26
CHAPTER 4: RESULTS AND DISCUSSION.....	32
4.1 Anisotropic effect	32
4.2 Strain rate effect.....	37
4.3 SOC effect	38
4.4 Charging rate effect	45
4.5 Cycling effect	61
4.6 Interfacial binder effect	69
CHAPTER 5: CONCLUSION	71

REFERENCES 73

LIST OF TABLES

TABLE 1: Details of the battery cycler used for charge/discharge of batteries	11
TABLE 2: Material properties: Young's modulus and density of the samples for different material orientations.....	23
TABLE 3: Material properties: Calculated yield stress and yield strain for different orientations and the materials at SOC=0.	23
TABLE 4: Density variation and density change for electrodes with increasing SOC with respect to thickness.....	26
TABLE 5: Summary of increase/decrease in strength of electrode samples with active material and current collector with various phenomenon.	61

LIST OF FIGURES

FIGURE 1: Illustration of 21700 LIB showing the layers of electrode and separator of jellyroll.	12
FIGURE 2: Illustration of initial charge/discharge cycling program.	14
FIGURE 3: Illustration of improved charge/discharge cycling program.	14
FIGURE 4: Illustration of charge/discharge cycle at SOC = 0, SOC = 0.2, SOC = 0.4 and SOC = 0.6 at 1-C charging rate	15
FIGURE 5: Illustration of: (a) current, (b) voltage fluctuations with charging/discharging cycles w.r.t. time	16
FIGURE 6: Illustration of battery cutting stages: (a) Battery sample with different SOC's (i.e. 0, 0.2, 0.4 and 0.6) out removed from cycler with 1C charging rate, (b) The battery mounted on the tool to cut off the battery cap, (c) The battery with the cap removed, (d) Anode covered with tape to avoid internal short circuit by accidental touching with cathode, (e) Shell cutting to remove the jellyroll, (f) Jellyroll after removing the shell.	17
FIGURE 7: From electrode rolls to testing samples (a) Anode Electrode roll separated from the jellyroll, (b) Cathode Electrode roll after separation from jellyroll and removal of separator, (c) Anode electrode flattened on the desk showing the orientation 0°, 45 and 90° in which the electrode will be sampled, (e) Anode samples cut out from the roll at 0°, (f) Cathode sample cut out from the roll at 0°	17
FIGURE 8: Illustration of the tensile testing experiment setup on Instron 3000 loading machine, Samples showing fracture after tensile test: (b) cathode electrode with active material for SOC=0 and orientation=0°, (c) anode electrode with active material for SOC=0 and orientation=0°, (d) cathode current collector for SOC=0 and orientation=0°, (e) anode current collector for SOC=0 and orientation=0°	19

FIGURE 9: Illustration of: (a) Young's modulus and yield calculation from stress-strain curves of anode current collector samples at SOC=0 and orientation=45°, (b) boundary conditions applied to the sample used in numerical simulation with mesh and dimension.....	22
FIGURE 10: Curve fit anode electrode in MATLAB for plastic stage at strain rate 1/s using Ramberg-Osgood model.....	28
FIGURE 11: Curve fit of anode electrode in MATLAB for plastic stage at strain rate 1/s using Johnson-Cook model.....	29
FIGURE 12: Stress vs strain comparison of anode current collector with simulation results showing contour plots at various instances from start of plastic stage to failure at SOC=0 along 0° for the following strain rates: (a) 0.01/s, (b) 0.1/s, (c) 1/s, (d) 10/s	31
FIGURE 13: Stress vs strain comparison of experiment and simulation curves at 0.01/s, 0.1/s, 1/s, 10/s strain rates along 0° for: (a) cathode electrode with active material at SOC=0, (b) anode electrode with active material at SOC=0, (c) cathode current collector at SOC=0, (d) anode current collector at SOC=0.....	34
FIGURE 14: Stress vs strain comparison of experiment and simulation curves at 0.01/s, 0.1/s, 1/s, 10/s strain rates along 45° for: (a) cathode electrode with active material at SOC=0, (b) anode electrode with active material at SOC=0, (c) cathode current collector at SOC=0, (d) anode current collector at SOC=0.....	34
FIGURE 15: Stress vs strain comparison of experiment and simulation curves at 0.01/s, 0.1/s, 1/s, 10/s strain rates along 90° for: (a) cathode electrode with active material at SOC=0, (b) anode electrode with active material at SOC=0, (c) cathode current collector at SOC=0, (d) anode current collector at SOC=0.....	35

FIGURE 16: Stress vs strain comparison with different strain rates for anode electrode with active material samples for different SOC along 45° with simulation results: (a) SOC=0, (b) SOC=0.2, (c) SOC=0.4, (d) SOC=0.6	35
FIGURE 17: Stress vs strain curves for anode electrode with active material samples comparing different SOC (i.e. 0, 0.2, 0.4 and 0.6) along 45° for strain rate of: (a) 0.01/s, (b) 0.1/s, (c) 1/s, (d) 10/s, for anode current collector samples comparing different SOC (i.e. 0, 0.2, 0.4 and 0.6) along 45° for strain rate of: (e) 0.01/s, (f) 0.1/s, (g) 1/s, (h) 10/s	39
FIGURE 18: Stress vs strain curves for cathode electrode with active material samples comparing different SOC (i.e. 0, 0.2, 0.4 and 0.6) along 45° for strain rate of: (a) 0.01/s, (b) 0.1/s, (c) 1/s, (d) 10/s, for cathode current collector samples comparing different SOC (i.e. 0, 0.2, 0.4 and 0.6) along 45° for strain rate of: (e) 0.01/s, (f) 0.1/s, (g) 1/s, (h) 10/s	41
FIGURE 19: Stress vs strain curves for anode electrode with active material for charging rates 0.1-C, 0.5-C, 1-C and 2-C at 1-cycle, SOC=0 for 0° samples.	42
FIGURE 20: Stress vs strain curves for cathode electrode with active material for charging rates 0.1-C, 0.5-C, 1-C and 2-C at 1-cycle, SOC=0 for 0° samples.	43
FIGURE 21: Stress vs strain curves for anode current collector for charging rates 0.1-C, 0.5-C, 1-C and 2-C at 1-cycle, SOC=0 for 0° samples.	43
FIGURE 22: Stress vs strain curves for cathode current collector for charging rates 0.1-C, 0.5-C, 1-C and 2-C at 1-cycle, SOC=0 for 0° samples.	44
FIGURE 23: Stress vs strain curves for anode electrode with active material for charging rates 0.1-C, 0.5-C, 1-C and 2-C at 10-cycle, SOC=0 for 0° samples.	46
FIGURE 24: Stress vs strain curves for cathode electrode with active material for charging rates 0.1-C, 0.5-C, 1-C and 2-C at 10-cycle, SOC=0 for 0° samples.	46

FIGURE 25: Stress vs strain curves for anode current collector for charging rates 0.1-C, 0.5-C, 1-C and 2-C at 10-cycle, SOC=0 for 0° samples.....	47
FIGURE 26: Stress vs strain curves for cathode current collector for charging rates 0.1-C, 0.5-C, 1-C and 2-C at 10-cycle, SOC=0 for 0° samples.....	47
FIGURE 27: Stress vs strain curves for anode electrode with active material for charging rates 0.5-C, 1-C and 2-C at 50-cycle, SOC=0 for 0° samples.....	48
FIGURE 28: Stress vs strain curves for cathode electrode with active material for charging rates 0.5-C, 1-C and 2-C at 50-cycle, SOC=0 for 0° samples.....	48
FIGURE 29: Stress vs strain curves for anode current collector for charging rates 0.5-C, 1-C and 2-C at 50-cycle, SOC=0 for 0° samples.....	49
FIGURE 30: Stress vs strain curves for cathode current collector for charging rates 0.5-C, 1-C and 2-C at 50-cycle, SOC=0 for 0° samples.....	49
FIGURE 31: Stress vs strain curves for anode electrode with active material for charging rates 0.5-C, 1-C and 2-C at 100-cycle, SOC=0 for 0° samples.....	50
FIGURE 32: Stress vs strain curves for cathode electrode with active material for charging rates 0.5-C, 1-C and 2-C at 100-cycle, SOC=0 for 0° samples.....	50
FIGURE 33: Stress vs strain curves for anode current collector for charging rates 0.5-C, 1-C and 2-C at 100-cycle, SOC=0 for 0° samples.....	51
FIGURE 34: Stress vs strain curves for cathode current collector for charging rates 0.5-C, 1-C and 2-C at 100-cycle, SOC=0 for 0° samples.....	51
FIGURE 35: Stress vs strain curve comparing number of cycles at 0.5-C, SOC=0, 0° for (a) anode electrode with active material, (b) cathode electrode with active material; (c) anode current collector, (d) cathode current collector	54

FIGURE 36: Stress vs strain curve comparing number of cycles at 1-C, SOC=0, 0° for

- (a) anode electrode with active material, (b) cathode electrode with active material;
(c) anode current collector, (d) cathode current collector56

FIGURE 37: Stress vs strain curve comparing number of cycles at 2-C, SOC=0, 0° for

- (a) anode electrode with active material, (b) cathode electrode with active material;
(c) anode current collector, (d) cathode current collector58

FIGURE 38: Force vs displacement curves at 1 cycle, 1-C charging rate, SOC=0

- comparing (a) anode electrode with active material and anode current collector, (b)
cathode electrode with active material and cathode current collector..... 60

LIST OF ABBREVIATIONS

ISC	Internal Short Circuit
SOC	State of Charge
NCA	Nickel Cobalt Aluminum
LIB	Lithium-ion Battery
FEM	Finite Element Modeling
E	Young's modulus
ρ	Density
σ_y	Yield stress
ε_y	Yield strain
σ_f	Failure stress
ε_f	Failure strain
ε_{pl}	Plastic strain
ε_0	Reference strain
A	Material parameter in Johnson-Cook model
B	Material parameter in Johnson-Cook model
C	Material parameter in Johnson-Cook model
L	Length of sample
W	Width of sample
T	Thickness of sample
CCC	Constant Current Charging
CCD	Constant Current Discharge

ANW	Anode with active material
CAW	Cathode with active material
ANWO	Anode without active material
CAWO	Cathode without active material
PP	Porous electrode polynomial
SP	Single Particle
P2D	Pseudo two-Dimensional
BTMS	Battery Thermal Management Systems
PFM	Phase Field Model

CHAPTER 1: INTRODUCTION

1.1. Background

The increasing population has eventually led us to the consumption of oil and fuel in abundance. As the reserves of the traditional non-renewable are depleting, the world is moving toward developing more reliable methods to keep the industries, vehicles, and much more working. The industrial revolution had used methods to increase manufacturing using more effective ways and resources at hand. The research put on centuries ago was the foundation of the advancements made all around the globe. With the increase in the use of traditional fuels, the residue and byproducts had a severe impact on the climate and the environment. Release of CO₂, greenhouse gases, emissions from vehicles, and industries had a noticeable contribution to environmental change[1-4]. To reduce the damage and have a safe and sustainable alternative to the mentioned resources, scientists and engineers aim at research for use and development of renewable energy sources (viz., wind, solar, hydro, and among others), and storage of the generated energy [1]. Storing the excess generated energy has always been a huge challenge. About three decades ago, the secondary battery was introduced to the world. Since then a lot of research work, including and not limited to improving capacity, energy efficiency, low cost, and user safety, has led to the development of advanced battery cells for commercialization [3, 5-7]. The battery converts chemical energy to electrical energy for use, and again, the generated power at the renewable power plants can be stored safely. Development of the rechargeable battery as per consumer demands has given a wide variety of cells used in a number of applications improving mobility, energy density, and much more [5, 8, 9]. Batteries have exceeded expectations and have emerged as a reliable option for the application not limiting to military, aerospace, commercial electronic devices, and among others [3, 10].

One of the most famous and widely used battery is lithium-ion based. lithium metal being a hazardous substance to use, its application was soon abandoned after its invention despite better electrochemical potential. Further development in the same sector showed combining lithium with other materials proved efficient hence lowering the risk of endangering the users[1, 11, 12].

1.2.Literature review

Previous work has reflected a detailed study of the internal battery components. It is investigated the lithium-ion battery (LIB) contains electrodes (containing active materials and current collectors) along with electrolyte which makes the ions transfer between electrodes. The process lithiation and de-lithiation or ion transfer can be explained as follows: The lithium ions move from cathode to anode via the electrolytic medium, while the electrons flow along the external wires associated. The process of the lithiation and de-lithiation of ions causes the active material to stress internally. These stresses under variable conditions may cause fractures, change in morphology of the active material resulting in the electrochemical performance of LIB, such as capacity decay and efficiency reduction [13-18]. The stresses generated on the active material particles differ with the application of variable charging rates, charge/discharge cycles, and the size of the active materials [19]. Due to a momentous impact on lithiation and de-lithiation process investigation of the kinematic and fracture mechanics on electrodes has helped in discovering the internal mechanism of the LIB with the help of mechanical properties, charging/discharging rates, cyclability, State of Charge (SOC) effects, strain rates effects [4, 20-23].

Abundant research has been conducted to categorize and explore the mechanical behavior of LIB. The stresses generated in LIB electrodes are majorly dependent on structural response, strain rate, SOC, charging rates, cyclability for the battery for

dynamic loading provides insights into the mechanical and electrochemical behavior of the LIBs [20, 21, 24-26]. 18650 battery cell research conducted by a number of groups with experiments and finite element modeling (FEM) simulations focusing on the electrochemical, mechanical behavior has led to an understanding of real-world scenarios. Modeling study considerations for the internal stresses include dynamics, kinematics, and thermal models that provide a vast perception of the internal working of the electrodes and LIBs [18, 27-29]. Battery research is mainly categorized into the following major categories: (1) battery cell and battery pack study, (2) microscale/microscopic (study related to the material of electrodes and optimization), and (3) mesoscopic study (the study of mechanical, thermal, kinematic behaviors of the battery and battery components)[30, 31].

The application of cylindrical LIBs in the battery packs for electric vehicles indicated the need for safety and reliability of the battery used. [20, 32] conducted a thorough macro structural and mechanical deformation study with the aid of FEM validated by mechanical abuse, e.g., radial compression, indentation, and three-point bending, nail penetration, pinch [27, 33-40]. To predict the load state and internal short-circuit (ISC), the authors studied the mechanical abuse over whole LIB (including jellyroll and casing), the mechanical model study of the stainless-steel casing of the battery, and the jelly roll with electrodes with active materials and separators [41, 42]. A drop test experiment and a validating numerical model simulation conducted by Avdeen et al. contributed to the insight for developing a design safe for catastrophic impact on electric vehicles in case of mishaps [35, 43]. Additionally, to improve the dynamic understanding of a model with SOC and strain rate dependency under bending, indentation, radial compression of LIBs predicting the mechanical behavior established a solid foundation to LIB safety design [20]. The tests indicated battery cell endures the

risk of thermal runaway irrespective of the size of deformation but is more related to the parameters like capacity and SOC [36]. In an unfortunate event like a crash, a single deformed battery cell is responsible for the failure of the battery pack. The arrangement, packing density, and battery connections (series or parallel) are also contributing factors in the failure and mishap. Liu et al. related the packing density, structural stiffness, with mechanical integrity of the pack delivering results with minimum failure by optimizing the packing models [44]. The combination of the experiments and numerical modeling or mathematical modeling help in the investigation of the ISCs and hence thermal runaway. These works have driven researchers in developing a battery management system (BMS) compatible to individual battery cell, battery pack, and even to the complete system. Application of the BMS has optimized performance and reduced failures [45].

A macro-mechanical FEM of the battery cell, can assist in anticipating the crashworthiness of other batteries for current and future research [32, 38]. Similar to the cylindrical LIB, a study with elliptical battery cell, pouch cells [34, 46], and mobile battery [36] cells under various loading scenarios by an investigation and development of micro-mechanical model provided an insight into the failure in multi-layered and multi-material structure of the battery cell. Mechanical abuse such as thickness compression, local punch indentation, and axial compression on the pouch cells with numerical simulations also assist the mechanical behavioral study as mentioned which provides a unique approach to uniform and non-uniform mechanical loading scenarios [15, 17, 47-50]. Battery penetration is another major cause of the short-circuit and thermal runaway. Detailed experimentation and computational simulation with 1-D battery model, 3-D failure model derived from Newman model for variable parameters during penetration, has stipulated a safety design for LIBs. The coupled mechanical-

electrochemical-thermal modeling and simulation has served as guidelines for safer battery design during crashes [39, 40, 51].

Microscale and macroscale understanding of the battery structure with material characterization showed a sequence of failure under mechanical abuse loadings due to compression, indentation, and tension [9, 52-54]. This investigation fueled the development of efficient and effective short-circuit models based on the results provided [14, 37, 55]. In association with the mentioned study, an approach on computational modeling on the different scales of the cell paved a path to a profound understanding of lithiation/de-lithiation, degradation, and dendritic growth of lithium on separators and electrodes. Modeling on multiscale eliminates the limiting factors analyzing the LIB [56]. Primarily to ensure passenger safety in case of crash, a multifunctionality study with FEM has proved beneficial in analyzing and advancing the damage tolerances and capacities for hybrid and completely electric vehicles [57].

This overall research conducted has provided a detailed matrix for OEM and EV manufacturers to develop a LIB that can sustain the real world harsh conditions and cause no harm to the end user ensuring safety.

In addition to the experimentation and numerical simulation, a thorough analysis of battery management systems (BMS) targeting key issues of batteries as voltage, SOC, state of health, and state of function for batteries in electric vehicles and battery performance has helped in the diagnosis of battery and provide inspiration to future work [4, 58]. The review summarizes the basic methods and procedures for any BMS and the specific area where attention is required for developing a better battery system and safe to use the battery model. Hannan et al. analyzed the challenges faced by researchers and automotive manufacturers in BMS methodology for the assessment of SOC and suggested a few solution to improve the present models and systems [4].

Along with the mentioned parameters, another concerning factor is the aging of the batteries in electric vehicles. Aging of LIB affects the performance irrespective of the use and is considered a difficult job with environmental factors, working conditions, and similar variables. Reference [59] reviewed mechanisms and estimated consequences on the automotive applications for aging with electrochemical mechanism, various methods to perform and analyze the aging with respect to current and voltage study, cycle aging, calendar aging, and analytical methods. A battery can be completely diagnosed if real-time estimations and development of an aging estimated model, demanding to focus on this study which will help in an improvised battery for the electric vehicle market.

18650 LIB being a prominent commercially used battery, research over cathode and anode is eminent for internal understandings of LIB. Golubkov et al. [60] tested various cathodes from 18650 LIB. The materials of cathode under study were as follows LiFePO_4 (LFP), $\text{Li}[\text{Ni}_{0.45}\text{Mn}_{0.45}\text{Co}_{0.10}]\text{O}_2$ (NMC), and a blend of LiCoO_2 and $\text{Li}[\text{Ni}_{0.50}\text{Mn}_{0.25}\text{Co}_{0.25}]\text{O}_2$ (NMC/LCO), respectively [61]. The electrode study has proved that any battery with excellent thermal properties of electrodes will substantially reduce thermal runaway following the ISC. Similar to the cathode, the anode electrode is as well a major contributing factor for internal short circuits [28, 62]. Active material on anode is also enhanced from graphite to Si and Sn-based composites providing better calendar life, increased capacity, and even faster charging rates [61, 63]. The development of new and improved battery components such as electrode materials, electrolytic solution, separators, and outer shell cases are demanding and vital. These advancements are directly associated to composition, morphology, material chemistry, electrochemical behavior, and thermal stability [9, 64]. A detailed analysis of crack propagation in active materials due to variable parameters as SOC and strain rate gives

an insight into the LIB and its electrodes [16, 65]. Phase-field models (PFM) coupling the stress evolution on material cracks due to lithiation provide an insightful and detailed analysis of LIB dynamics and failure mechanisms [66]. Active materials are bonded to the current collectors with the help of adhesive. These electrodes are basically a sandwich structure with a current collector in-between active material coat [26, 62]. Considering the structure of electrodes, the bonding between active materials and current collectors is significant as it contributes to the overall strength of electrodes [67]. Hence, these adhesion and cohesion properties and failure tests help in the development of structurally strong yet effective material for electrodes. Experiments conducted in [60] show promising results validating the claim of selecting the best cathode electrode based on the manufacturing process and the manufacturing material used. Anode and cathode of LIBs with variable SOC and variable strain rates comparing the experimental results and the mechanical model results for a tensile test showed there was a variation in stiffness and strength of anode electrode as compared to cathode electrode [26, 62]. The study of the anode and cathode depending on the SOC and state of health (SOH) as the major factors affecting the behavior of LIB delivers an engaging approach and has proved to be a hot topic of interest in researchers. The coupling of these two factors and their behavior affecting failure stress and failure strain was investigated, revealing their influence on temperature and stiffness of the electrodes.

As mentioned, the anode and cathode of lithium-ion batteries are the most prominent components. Thus, an understanding of the mechanical behavior, failures of these electrodes are significant for the safety of LIBs. Testing of electrodes (i.e., anode and cathode) with experiments until failure, along with numerical computational modeling, was conducted following the prior insights [22, 68]. This research reveals that as an initial stage for the development of multiphysics and failure prediction

models. Apart from the electrodes (i.e., anode and cathode), separators used in the LIB are as well one of the principal components responsible for the vivid behavior of the battery cell. The separators keep the battery from getting short-circuit and provide structural support to the battery cell. Jiang et al. explored the mechanical behavior of anode, cathode, anode current collector, cathode current collector, and the separator of LIB [69]. Authors introduced the tensile testing to investigate the mechanical behavior which revealed strain rate and anisotropy dependence characteristics of electrodes and separator [70]. Furthermore, creep tests and dynamic mechanical behaviors of the separators in LIBs elucidated the viscoelasticity by the viscoelastic model [21]. The strain rate dependence was also observed from 0.01/s to 50/s. The development of separators such as ceramic and polymer composite material separators has unveiled advantages with durability, thermal stability making them safety attested [41, 64].

Along with the mechanical model behavior study, researchers focus on a keen investigation of other phenomenon and models such as three-dimensional mechanical, electrical, and thermal coupled multiphysics model, short-circuit model, exothermic model. A systematic multiphysics approach to couple these mentioned models to deliver a framework for advanced battery and electric vehicle design at particle and electrode level was introduced and developed [23, 31, 71]. The literature discusses the progression of LIB under mechanical abuse to ISC for different states of charges and coupling the mechanical-electrical-thermal models to evaluate the complicated multiphysical nature of lithium-ion batteries [39].

With the material study on the electrodes, it is necessary to have a detailed study of the LIB on the microscopic and mesoscopic level. Mathematical modeling is considered a safe option to work on these behavioral studies as the risk of working on hazardous materials of LIBs is reduced [72, 73]. These studies provide a deeper

understanding of the lithium-ion batteries to tackle problems related to charging rates, SOC effects, capacities, and thermal runaways [72]. Taking the cycling and aging of batteries into consideration, numerical simulations can predict the battery life (battery calendar life) to a certain extent [74]. In addition, the fatigue of battery electrode due to aging and cycling, temperature variation caused by voltage/current change during charging/discharging, overcharging will also have an impact on the battery life and its electrochemical stature [75-77]. A study by Barai et al. with 1D and 2D models revealed that a reduction in degradation of LIB capacity is possible with careful modeling of electrodes [19]. To correlate the functioning of the LIB PP model, i.e., porous electrode polynomial approximation model, SP model i.e., the single-particle model and the P2D, i.e., the pseudo two-dimensional model provide better results with low computational/simulation time but with a better accuracy over the traditional battery models [78, 79].

These various model parameters coupled together with a computational framework for cylindrical battery considering mechanical behavior and particle interactions can bridge the gap of various coupling phenomenon of LIBs [23, 31, 80]. Multiphysics modeling explains the overall mechanism of LIB working with a minor variation in any parameter. The LIBs are modeled in a homogenous way while still capable of delivering simple and satisfactory results. A detailed numerical simulation depending on the requirement of the study is drafter. LS-Dyna and ABAQUS are the two most famous simulation tools used worldwide for the evaluation of the batteries and electrodes [20, 47, 81]. Researchers have introduced and worked upon the mechanical model, battery model, short-circuit model, exothermic model, and thermal model together post ISC in the battery.

In summary, the factors leading a LIB to thermal runaway are both internal and external. Mechanical abuse being leading cause of mishaps in real world scenario, a comprehensive understanding in relation with internal contributing parameters can improve the vehicle or application reliability and efficiency. Exploring the unclear mechanics has assisted in advancing a safer battery to be used in varied applications.

1.3.Objective

Even though the literature provides numerous investigations targeting safety issues with lithium-ion batteries, including and not limited to studies on numerical modeling and experiments on battery cell, battery module, and battery packs; however, fundamental multiphysics response of the battery still has not been revealed and understood yet. As mechanical loading is a responsible factor for the ISC which proceeds to the electrochemical changes and hence the thermal runaway, predicting the battery behavior under numerous conditions is of utmost importance for safe use and application of the LIBs.

21700 LIB, as a next-generation of 18650 cells, are increasingly popular in engineering applications. With the larger and higher energy density of the cells for 21700 cells, the mechanics-chemo-electrochemical behaviors upon mechanical abusive loading are expected to be significantly different. To explore the possible LIB behaviors, in this thesis, the mechanical behaviors of the anodes and cathodes have been fully characterized by consideration of the anisotropy, strain rate effect, SOC effect, charging rate, and cycling effects. Also, the experiments and numerical modeling conducted in this study with a detailed analysis method will be used for an in-depth understanding of mechanical deformation and failure mechanisms affecting the LIB performance.

CHAPTER 2: EXPERIMENTAL METHODOLOGY

The lithium-ion battery used in this study is a 21700 M50 LIB with a capacity of 5000 mA. The battery cycler characteristics and details are mentioned in Table 1. As mentioned in the literature review and background of the LIBs, the 21700 LIB cell has the same structure as that of other comparable commercial LIBs. The battery contains a steel casing wrapped in a plastic cover. The steel casing consists of a case surrounding the jellyroll and closed in with a steel cap to ensure the safety of the jellyroll. The jellyroll consists of layers as anode, separator, cathode, and separator rolled and stacked in this particular way. An illustration of the internal structure of 21700 battery is given in Figure 1.

2.1. Cycling methodology and procedure for the experiment

Table 1: Details of the battery cycler used for charge/discharge of batteries.

Sr. No.	Specification	Details
1	Model	CT6001A
2	Current range (A)	30A/60A/100A/120A/200A/300A/400A/480A
3	Voltage range (V)	5V
4	Working mode	Constant current charge and discharge, constant voltage charge and discharge, constant current and constant voltage charge and discharge, constant current and constant voltage discharge, constant power charge and discharge, constant resistance discharge, DCIR, rate charge, and discharge. Figure 5 represents the charge/discharge current and voltage.
5	Limit condition	Time, voltage, current, capacity, $-\Delta V$ and nearly 20 kinds
6	Protection conditions	Overvoltage, under voltage, overcurrent, undercurrent, overcharge capacity, over-discharge capacity and other
7	Programming steps	Not limited

Table 1: Details of the battery cycler used for charge/discharge of batteries.(continued)

8	Number of channels	1/2/4/8/16
9	Input impedance	$\geq 1\text{M}\Omega$
10	Output mode	Four electrodes (support reference electrode test)
11	Voltage accuracy	$0.05\%RD \pm 0.05\%FS$ (Control and detection)
12	Current accuracy	$0.05\%RD \pm 0.05\%FS$ (control and detection)
13	Constant power/constant resistance accuracy	$0.2\%RD \pm 0.2\%FS$ (control), $0.1\%RD \pm 0.1\%FS$ (measurement)
14	Computer system time	± 1 Seconds (without cumulative error)
15	Voltage resolution	With five significant digits (automatic)
16	Current resolution	With five significant digits (automatic)
17	Power supply	AC380V 50HZ Input power 2.4KW (single module)
18	Charging efficiency	$\geq 85\%$
19	Feedback efficiency	$\geq 70\%$
20	Protection level	IP20
21	Specification size single module	550mm(width)*432mm(depth)*165mm(height)

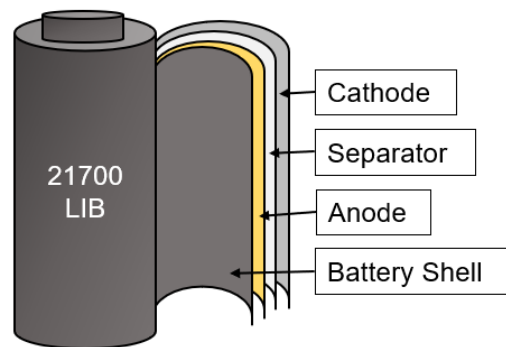


Figure 1: Illustration of 21700 LIB showing the layers of electrode and separator of jellyroll.

The cycler charges and discharges the batteries to replicate the working conditions as they are in the commercial applications. The experimental study conducted here in this thesis includes the charging and discharging of batteries for 1 cycle, 10 cycles, 50 cycles, and 100 cycles. Each of these cycles is conducted for the

charging rate of 0.1-C, 0.5-C, 1-C, and 2-C. The effect of the cycling performance, along with the charging rate performance, is investigated. In addition to this investigation the batteries with different State of Charges (SOCs) (i.e., 0, 0.2, 0.4 and 0.6) for 1 cycle at 1-C charging rate for orientations of 0° , 45° and 90° are also examined for the electrochemical behavior of the 21700 LIBs under mechanical abusive loadings.

For each condition combination of parameters namely SOC, charging rate, the number of cycles, a program is drafted to receive the desired charging and discharging situation needed. The detailed flow of these programs is given in Figure 2, Figure 3, and Figure 4. Initially, the batteries received from the manufacturer are 30% charged (i.e., SOC 0.3). The first step of these programs was to completely discharge the batteries to a SOC = 0. After they were charged to SOC=1 and then discharged to SOC=0, this process was considered as 1 cycle. A constant current charge and constant current discharge were applied. Considering that the 21700 LIB has 5000 mA capacity, the 1-C charging rate has 5000 mA current, 2- charging has 9999 mA current, 0.5-C charging rate has 2500 mA current, and 0.1-C charging rate has 500 mA current used for the process. As per the datasheet provided by the battery manufacturer, the maximum voltage that can be used is 4.2 V, and the cutoff voltage is 2.5 V was used as the limiting factor for programming. Charging with different charging rates has given the variation in the voltage of the batteries which has affected the mechanical properties such as the stress and strain post mechanical abusing. To get an even and approximate voltage values for all the batteries with different charging rates and the number of cycles, a resting case for about 1 hour was introduced in the program and followed by a further discharge with 100 mA as shown in Figure 3. Since the batteries were charged and discharged with constant current, the discharge with a smaller current facilitates the approximation in the voltages of these various batteries.

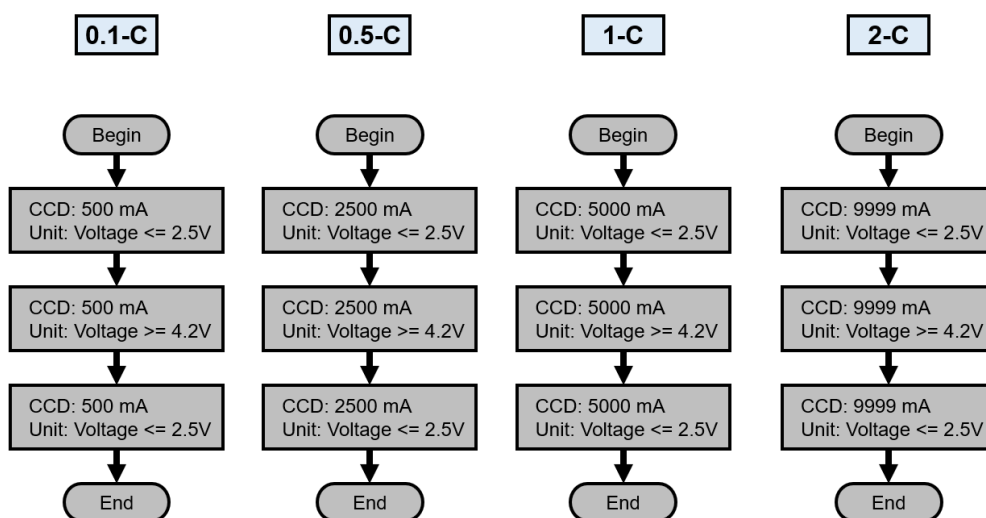


Figure 2: Illustration of initial charge/discharge cycling program.

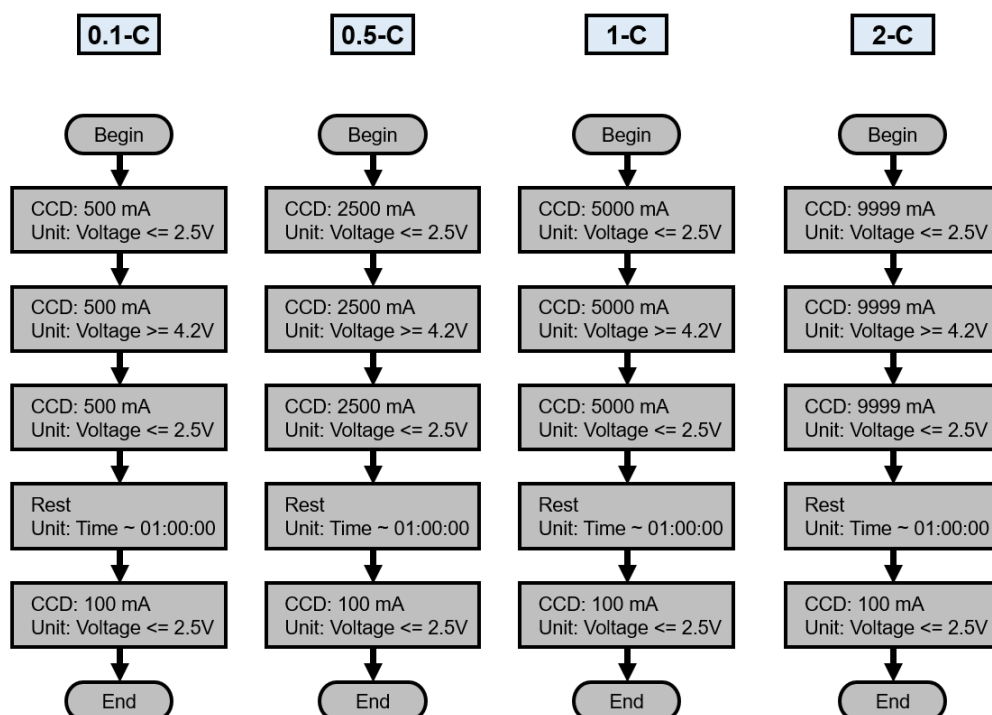


Figure 3: Illustration of an improved charge/discharge cycling program.

For determining the SOC of the battery with a 1-C charging rate, it was observed that the LIB took up 1 hour to charge up to SOC=0 and 1 hour to discharge to SOC=0. So, for 10% charging i.e., SOC=0.1, the battery needs 6 mins to charge. Hence for SOC=0.2 battery was charged for 12 mins after complete discharge, for SOC=0.4

battery was charged for 24 mins and for SOC=0.6 the battery was charged for 36 mins.

A detailed program flow is given in Figure 4.

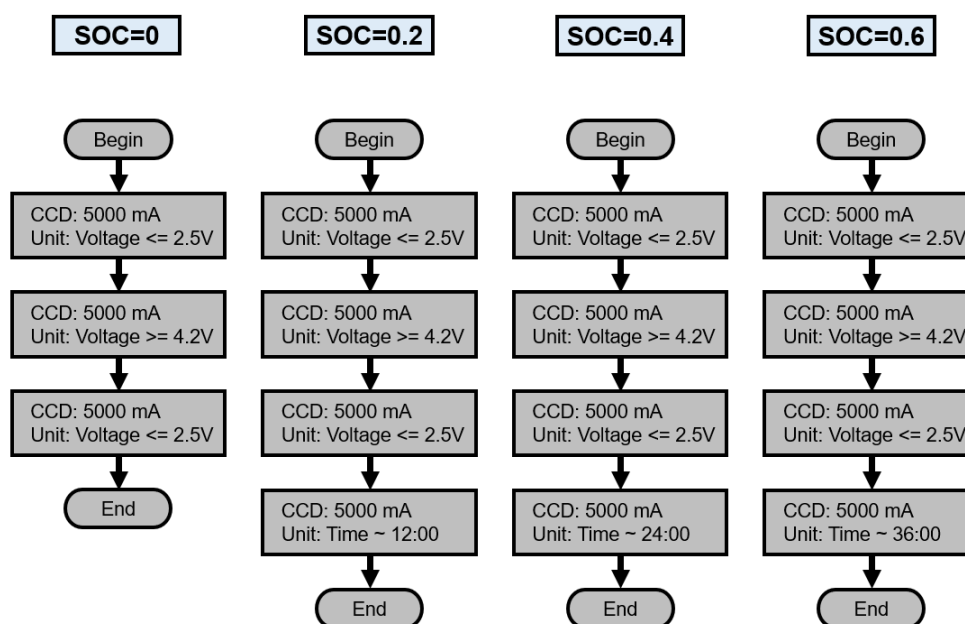


Figure 4: Illustration of charge/discharge cycle at SOC = 0, SOC = 0.2, SOC = 0.4 and SOC = 0.6 at 1-C charging rate.

2.2 Tensile testing procedure

Followed by the cycling, cells were disassembled, separating anode, cathode from the jellyroll to be sampled and measured for the tensile testing on the INSTRON machine, as shown in Figure 7. The process of battery disassembly started with cutting open the cap of the battery with the special cutter tool shown in Figure 6(b). The battery shell made of stainless-steel was cut using the pliers and removed. The samples cut out from the jellyroll were in three angle orientations 0° , 45° , and 90° . The 0° orientation is the machine direction, 90° is the rolling direction of the anode and cathode. And the 45° orientation is exactly midway between these two orientations. The sample was loaded in the INSTRON E3000 machine for the tensile testing. Tensile experiments for all samples were performed on the INSTRON E3000 machine with maximum dynamic loading of 3 kN, static loading of 2.1 kN, and $\pm 0.5\%$ indicated load accuracy. The

electrodes and current collectors were tested for four strain rates, i.e., 0.01/s, 0.1/s, 1/s, and 10/s. For each strain rate, three repeated tests were conducted to ensure consistency in the results. Each electrode was cut down for 12 samples in each case and each orientation. Hence for a particular battery anode, cathode, and their current collectors, 12 samples each were extracted and tested. For a sampling of the current collectors, the anode and cathode were cleaned with 70% ethyl alcohol with tissue paper for removing the active material off the electrodes. A detailed illustration of how the sample was loaded in the INSTRON E3000 is shown in Figure 8(a). The samples were fabricated 50 mm to 60 mm in length and 5 mm to 6 mm in width. Each sample was measured and tested to obtain accurate results.

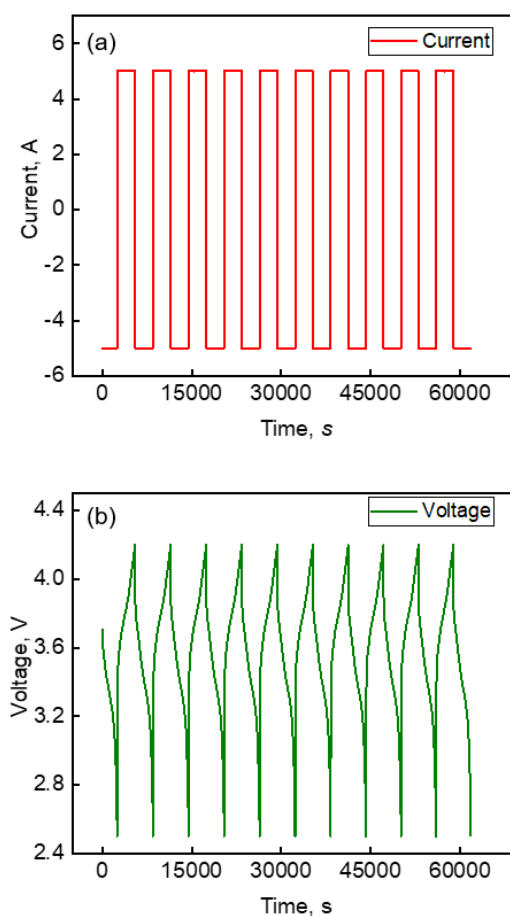


Figure 5: Illustration of: (a) current, (b) voltage fluctuations with charging/discharging cycles w.r.t. time.

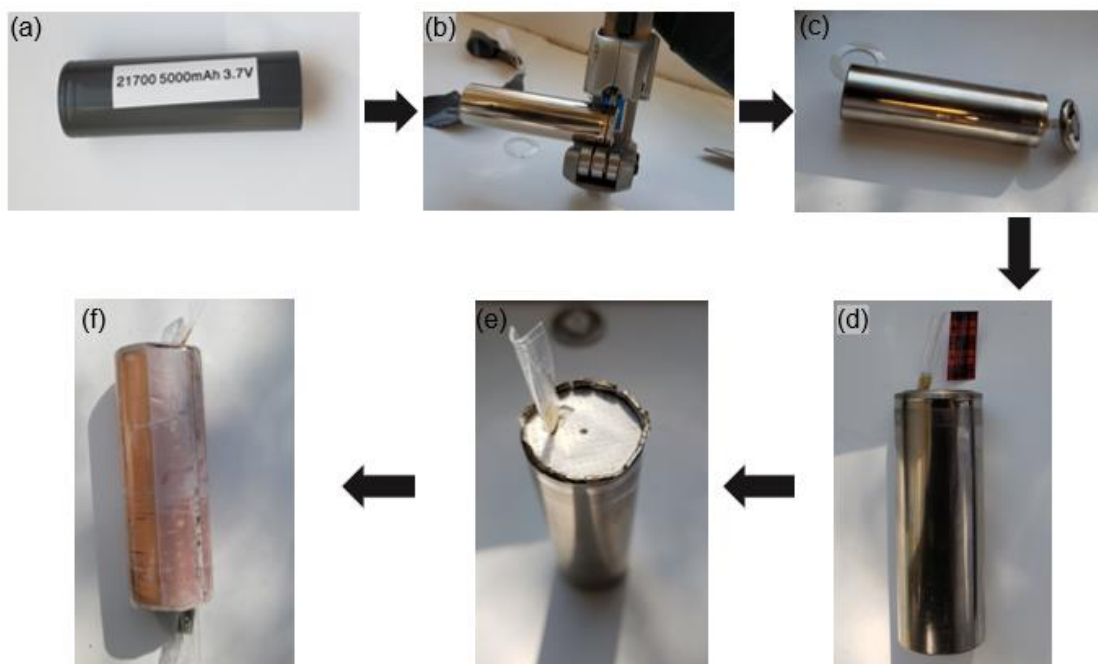


Figure 6: Illustration of battery cutting stages: (a) Battery sample with different SOCs (i.e., 0, 0.2, 0.4 and 0.6) out removed from cyclers with 1C charging rate, (b) The battery mounted on the tool to cut off the battery cap, (c) The battery with the cap removed, (d) Anode covered with tape to avoid ISC by accidental touching with the cathode, (e) Shell cutting to remove the jellyroll, (f) Jellyroll after removing the shell.

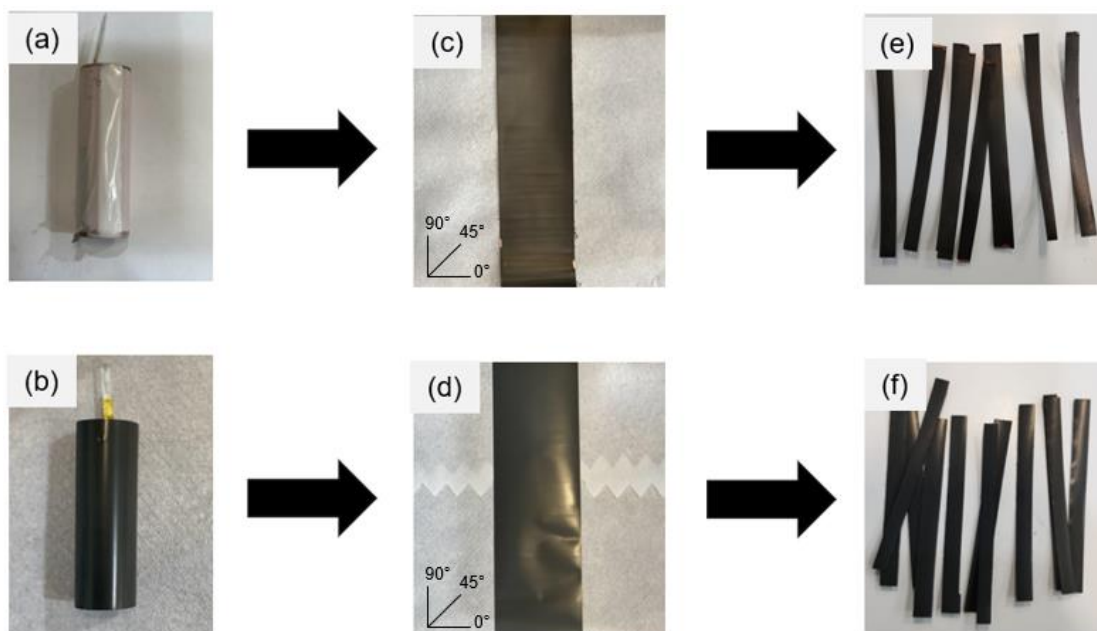


Figure 7: From electrode rolls to testing samples (a) Anode Electrode roll separated from the jellyroll, (b) Cathode Electrode roll after separation from jellyroll and removal of the separator, (c) Anode electrode flattened on the desk showing the orientation 0° , 45° and 90° in which the electrode will be sampled, (e) Anode samples cut out from the roll at 0° , (f) Cathode sample cut out from the roll at 0° .

Samples had shown variation in the thickness which was documented. Variation in the thickness of the electrodes and the current collectors has shown a huge impact on the stress-strain curves of the tensile test. Figure 8(b)-(e) show the electrode and current collector samples after the tensile test. The variation in thickness is caused by the lithiation and de-lithiation. Each strain rate used has a unique loading velocity. Considering the average length of the sample to be 40 mm, the loading velocities were 0.4 mm/s, 4 mm/s, 40 mm/s and 400 mm/s, for strain rates of 0.01/s, 0.1/s, 1/s, and 10/s.

A similar process of sampling and testing was implemented for all the batteries. Comparison of the results with different strain rates, SOC, charging rate, angle orientation, and the number of charging/discharging cycles for the stress-strain curves was plotted.

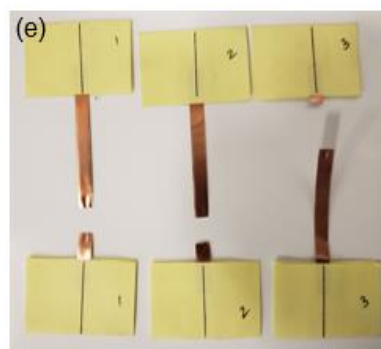
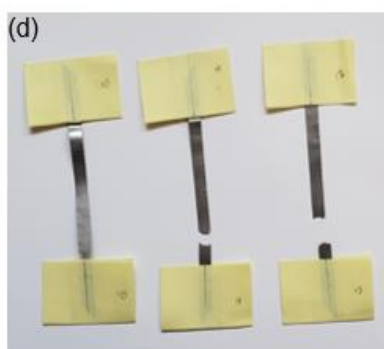
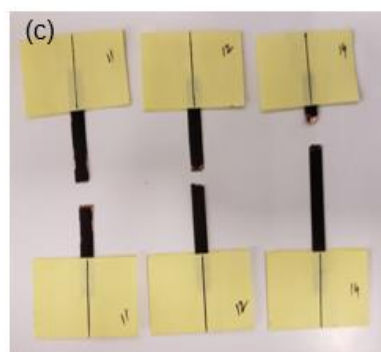
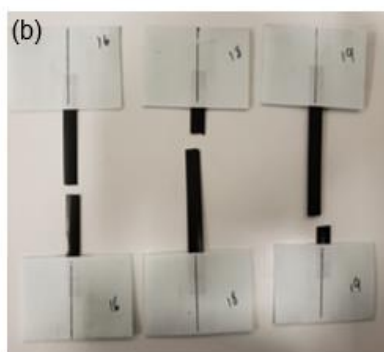
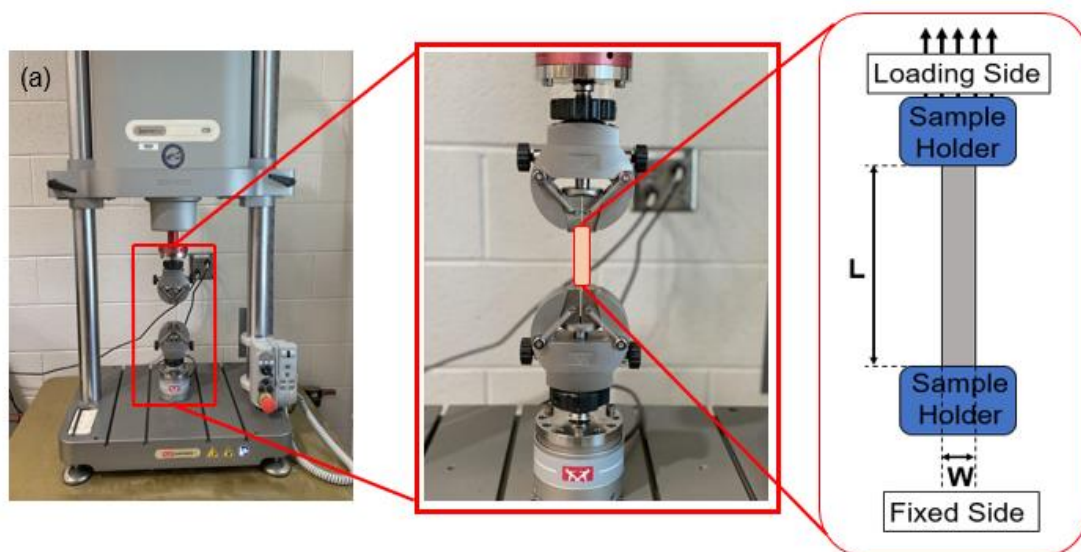


Figure 8: (a) Illustration of the tensile testing experiment setup on INSTRON 3000 loading machine, Samples showing fracture after tensile test: (b) cathode electrode with active material for SOC=0 and orientation=0°, (c) anode electrode with active material for SOC=0 and orientation=0°, (d) cathode current collector for SOC=0 and orientation=0°, (e) anode current collector for SOC=0 and orientation=0°.

CHAPTER 3: SIMULATION METHODOLOGY

3.1. Material properties and simulation module

To supplement the study of mechanical behaviors, we consider a numerical simulation approach to explore the electrode behavior under tensile testing. ABAQUS was used as the numerical simulation platform. Anode, cathode, and current collectors have different material properties. Considering the repeatability of the test for each strain rate (i.e., 0.01/s, 0.1/s, 1/s, 10/s) the material properties for one battery would be the same. The properties for the different orientation of the battery would be different, due to the manufacturing orientation. Also, with changing SOC, the properties may vary. These different properties of the electrodes and current collectors are detailed in Table. The yield stress and strain for different orientations are calculated given in Table 3. These properties were calculated and determined from the experimental stress-strain curves obtained from the experiment. Material properties such as young's modulus, density, stress, and strain were calculated with the help of force and displacement data extracted after the tensile testing of each sample. A slight variation in the density of the materials of different batteries was observed with less than 7% change in the value of density. Table shows the increase in the density value with increasing SOC for the anode and a decrease in density for cathode which also supports the claim of lithiation and de-lithiation.

Since the variation in density is not obvious, a standard mean value of density for the anode, cathode, and respective current collectors was chosen from the literature. This minute change did not have any significant change in the results of the simulation. The calculated Young's moduli of the current collectors, which are metals (i.e., copper and aluminum) are lower than those bulk materials. As the manufacturing of the current

collector is a malleability process, which changes the property of the metal. For the anode current collector, thin sheets used in LIBs have the young's modulus calculated as around 40-50 MPa, whereas the young's modulus of bulk copper is 120 Mpa. Similar variation in modulus was observed in this study as Young's modulus calculated was 29.3 Mpa [82].

Numerical simulation provides a deep and clear understanding of how the sample behaves under tensile loading, the hotspots where the stress is maximum, and where they fail. ABAQUS is a very powerful tool that can give an insight into the principal stress, von mises stress, unidirectional forces, and respective displacement and strains as needed for the sample. Model design in ABAQUS for the sample is illustrated in Figure 9(b), a single part was used to replicate the sample structure. The electrodes are multi-layered structures manufactured as the current collector sandwiched in between two layers of active material. For simplicity of the model, a homogeneous material property was considered. The elastic stage is set with respective modulus and standard poissons ratio value 0.3, while the plasticity stage uses the plastic stage data from the governing equation. The ductile failure stage is set as triaxiality 0.33, failure displacement 0.003 with strain rate dependent failure strain values.

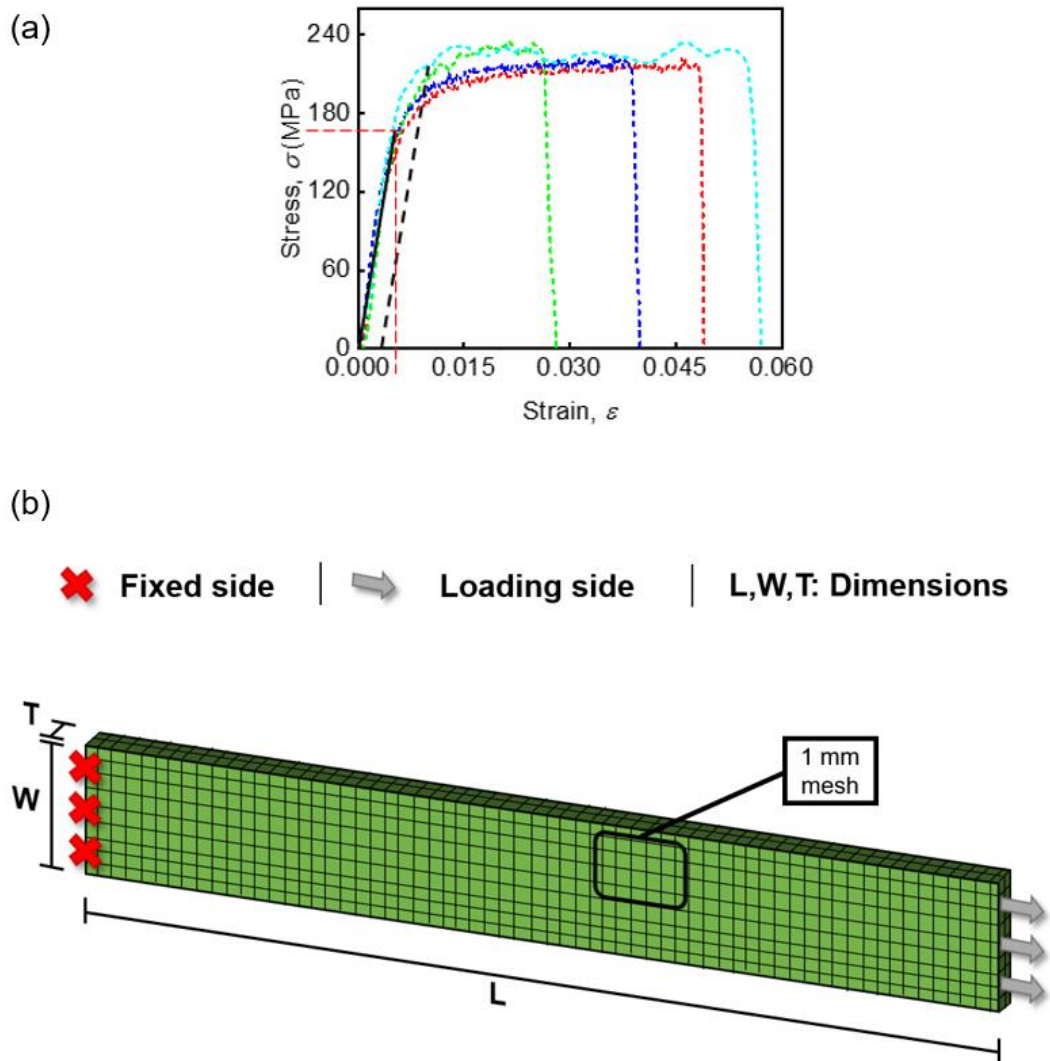


Figure 9: Illustration of: (a) Young's modulus and yield calculation from stress-strain curves of anode current collector samples at SOC=0 and orientation=45°, (b) boundary conditions applied to the sample used in numerical simulation with mesh and dimension.

Table 2: Material properties: Young' s modulus E and density ρ of the samples for different material orientations.

Sample	Cathode with active material	Anode with active material	Cathode current collector	Anode current collector	Anode with active material	Anode with active material	Anode with active material
SOC	0	0	0	0	0.2	0.4	0.6
<hr/>							
0°	Modulus (E) (Mpa)	4819.423	3327.66	31364.877	20406.536	--	--
	Density (ρ) (kg/m ³)	2890	1640	2700	8930	--	--
<hr/>							
45°	Modulus (E) (Mpa)	3003.39	3719.46	27999.005	29282.305	3339.13	6673.575
	Density (ρ) (kg/m ³)	2890	1640	2700	8930	1640	1640
<hr/>							
90°	Modulus (E) (Mpa)	3994.851	2718.84	26408.218	30912	--	--
	Density (ρ) (kg/m ³)	2890	1640	2700	8930	--	--

Table 3: Material properties: Calculated yield stress σ_y^q and yield strain ϵ_y^q for different orientations and the materials at SOC=0.

Anode with active material		Cathode current collector				Anode current collector				
	1/s	10/s	0.01/s	0.1/s	1/s	10/s	0.01/s	0.1/s	1/s	10/s
11.281	13.855	15.988	121.5037	132.46	135.4029	156.6249	165.8093	200.1748	216.2781	251.629
0.00324	0.00362	0.00378	0.00503	0.00386	0.00281	0.00263	0.00964	0.01481	0.00972	0.01294
16.139	17.501	20.5227	96.557	103.1357	113.2091	131.8764	167.211	182.5578	180.9328	200.4761
0.00563	0.00516	0.0068	0.00457	0.00499	0.00568	0.00671	0.00661	0.00671	0.00547	0.0051
17.579	18.3974	20.1023	62.535	109.5349	121.8785	146.866	151.7643	200.0828	206.314	220.0688
0.00973	0.01171	0.00548	0.00333	0.00552	0.00538	0.00513	0.00638	0.01075	0.00903	0.01171

Table 3: Material properties: Calculated yield stress σ_y and yield strain ϵ_y for different orientations and the material at SOC=0. (continued)

Samples	Cathode with active material					
	0.01/s	0.1/s	1/s	10/s	0.01/s	
Strain rate						
0°	Yield stress, (σ_y) (Mpa)	18.77	21.56	23.78	24.681	11.107
	Yield strain, (ϵ_y)	0.00744	0.00476	0.00484	0.00498	0.00384
45°	Yield stress, (σ_y) (Mpa)	20.1622	22.2403	22.9385	24.0393	15.1654
	Yield strain, (ϵ_y)	0.00797	0.00921	0.00965	0.00581	0.00565
90°	Yield stress, (σ_y) (Mpa)	15.456	18.599	20.4284	22.3522	14.304
	Yield strain, (ϵ_y)	0.00506	0.00631	0.00686	0.00662	0.00563

Table 4: Density variation and density change for electrodes with increasing SOC with respect to thickness.

SOC	Density ρ (kg/m ³)		Change in density Anode	Change in density Cathode
	Anode	Cathode		
0	$\frac{m_a}{(L*W*0.000198)}$	$\frac{m_c}{(L*W*0.000167)}$	-	-
0.2	$\frac{m_a}{(L*W*0.000203)}$	$\frac{m_c}{(L*W*0.000173)}$	2.46 %	3.46 %
0.4	$\frac{m_a}{(L*W*0.000205)}$	$\frac{m_c}{(L*W*0.000171)}$	3.41 %	2.33 %
0.6	$\frac{m_a}{(L*W*0.000211)}$	$\frac{m_c}{(L*W*0.000167)}$	6.16 %	0 %

3.2. Governing equations and model setup

The equation used for governing the plasticity stage is the Johnson-Cook model. Several equations were considered that could provide very reasonable and close results with the experimental plasticity values, such as, Mechanical Threshold Stress (MTS) model, Ramberg-Osgood Model. The MTS model had complexities with parameters that cannot be related to the electrode samples of LIBs. A detailed Johnson-Cook model and the Ramberg-Osgood model were referred to, and the equations are given as follows:

Eq. (1) is the general form of the Ramberg-Osgood model equation which is modified to the strain rate dependent Ramberg-Osgood plasticity model equation as mentioned in Eq. (2)

$$\varepsilon = (\sigma / E) + (K * [\sigma / E]^n)^{\frac{1}{n}} \quad \text{Eq. (1)}$$

$$\varepsilon = (\sigma / [E(1 + C * \ln(\varepsilon_{pl} / \varepsilon_0))]) + \{ K * (\sigma / [E(1 + C * \ln(\varepsilon_{pl} / \varepsilon_0))])^n \} \quad \text{Eq. (2)}$$

where ε is the strain, σ is the stress, E is the calculated young's modulus, ε_{pl} is the plastic strain rate, ε_0 is the reference strain rate, K and n are the hardening behavior

of the material and C is the material parameter. $\frac{\varepsilon_{pl}}{\varepsilon_0}$ is a dimensionless parameter

where the ε_{pl} changes as the strain rates.

Eq. (3) is the general form of Johnson-Cook equation which is modified to the strain rate dependent Johnson-Cook plasticity model equation, as mentioned in Eq. (4).

$$\sigma = [A + B * (\varepsilon_{pl})^n] \quad \text{Eq. (3)}$$

$$\sigma = [A + B * (\varepsilon_{pl})^n] [1 + C * \ln(\varepsilon_{pl} / \varepsilon_0)] \quad \text{Eq. (4)}$$

where σ is plastic stress, ε_{pl} is the plastic strain, ε_0 is reference strain, A , B , C , and n are material parameters. The ratio ($\frac{\varepsilon_{pl}}{\varepsilon_0}$) is a dimensionless parameter where

the plastic strain is changed as needed. The reference strain used in the simulation and MATLAB code is 0.01 s^{-1} .

The Ramberg-Osgood model can predict reasonably well, but it fails at higher strain rates. On the other hand, the Johnson-Cook model performs a good job in describing stress-strain curves at various strain rates, shown in Figure 10 and 11 and thus, we will choose Johnson-Cook model here. As there are too many data points, and the calculation is complex, MATLAB was used to compare the experimental data plasticity curve and the data extracted from the Johnson-Cook model equation. Data from the experiment was the input to get the plasticity curve per the Johnson-Cook model.

For the contact module, as there is just one part used in the simulation, no contact was assigned. To obtain the detailed output from each section of the model, a fine mesh of 1 mm was used. With no longer delay in the computational speed, the simulation gave out satisfactory and accurate results. The element type used in the

numerical simulation was C3D8R. The number of elements changed from sample to sample as the part was modeled for various battery samples of electrodes and corresponding current collectors. The boundary conditions set up is illustrated in Figure 9(b) as shown in the figure, one side was fixed without any movement, and the opposite side was restricted to have any movement except just for in one direction of loading to avoid twisting and other loading cases during the simulation. The boundary condition was common throughout all the samples. Loading condition is given by input for the displacement of the free end. Dynamic/explicit algorithm is selected in the simulation to get a better conversion at the end of the numerical simulation. To maintain a quasi-static loading condition, minimum kinetic energy is maintained during loading. The total time input during the initial and loading step was 0.01 s. Figure 12(a)-(d) shows a detailed illustration of how the sample behaves during the loading at different instances.

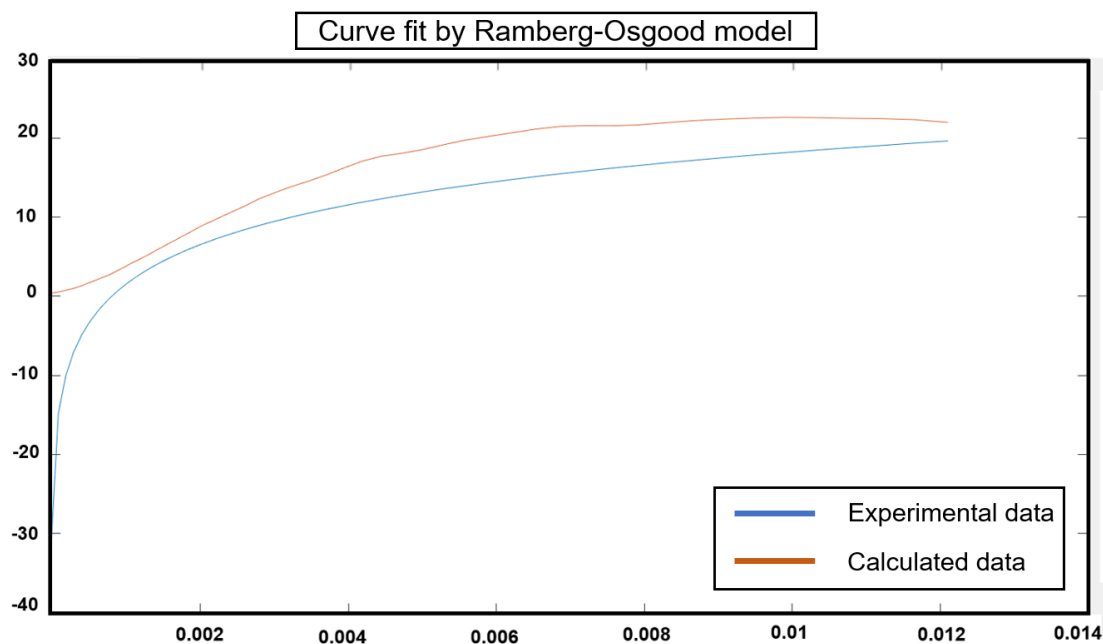


Figure 10: Curve fit of anode electrode in MATLAB for plastic stage at strain rate 1/s using Ramberg-Osgood model.

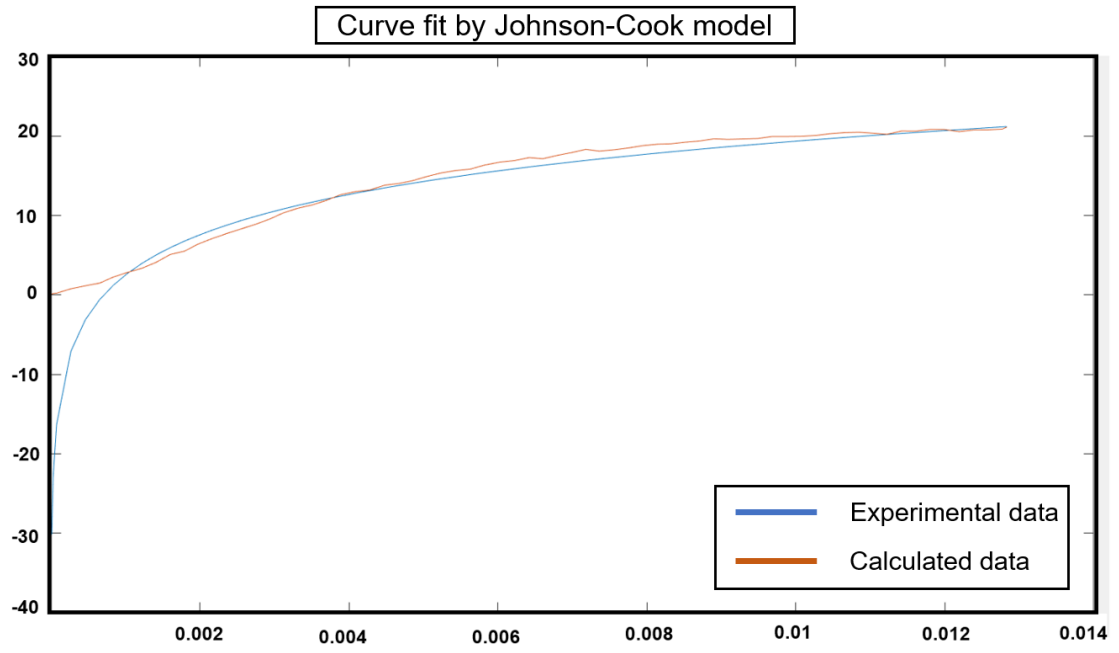
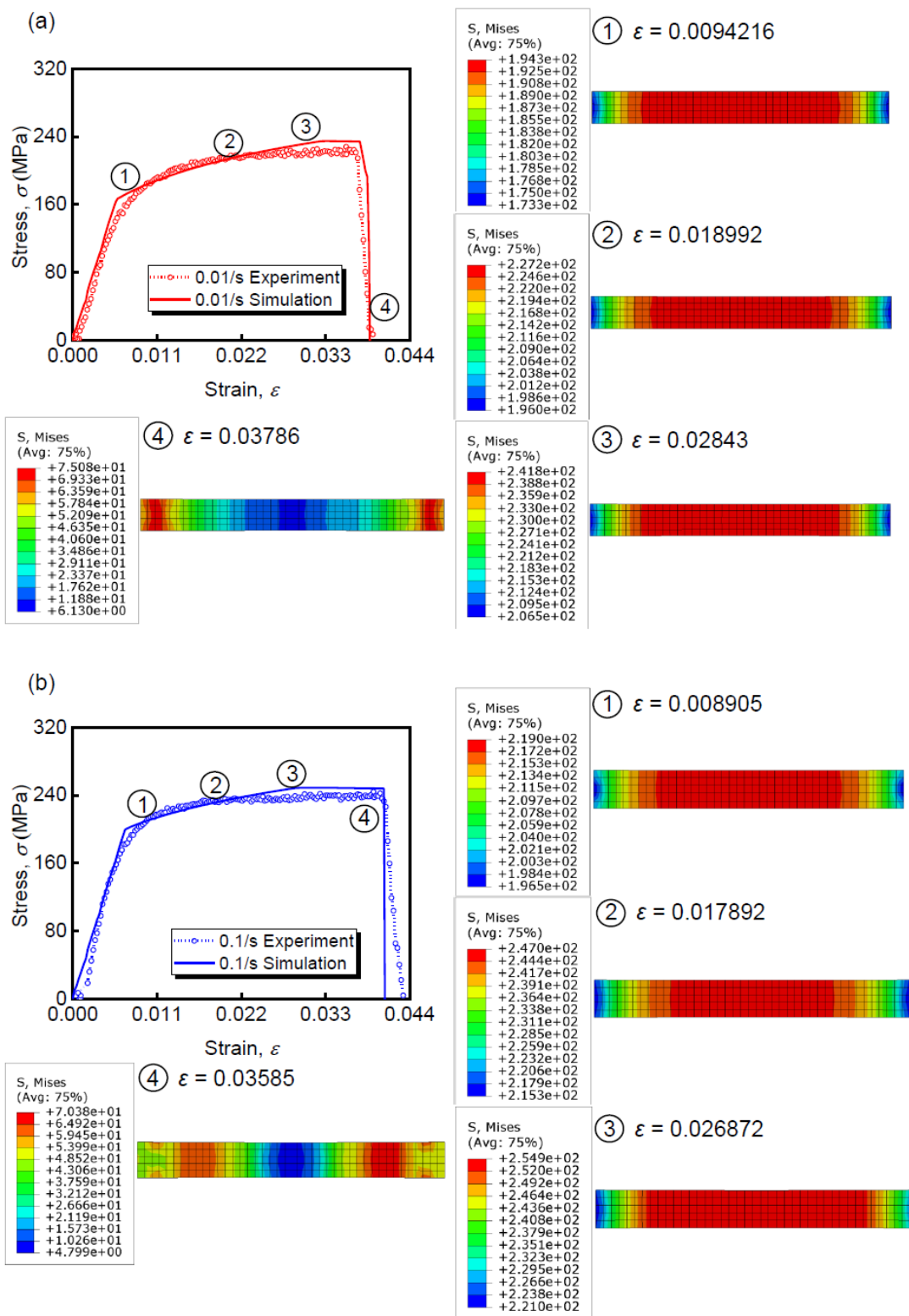


Figure 11: Curve fit of anode electrode in MATLAB for plastic stage at strain rate 1/s using Johnson-Cook model.



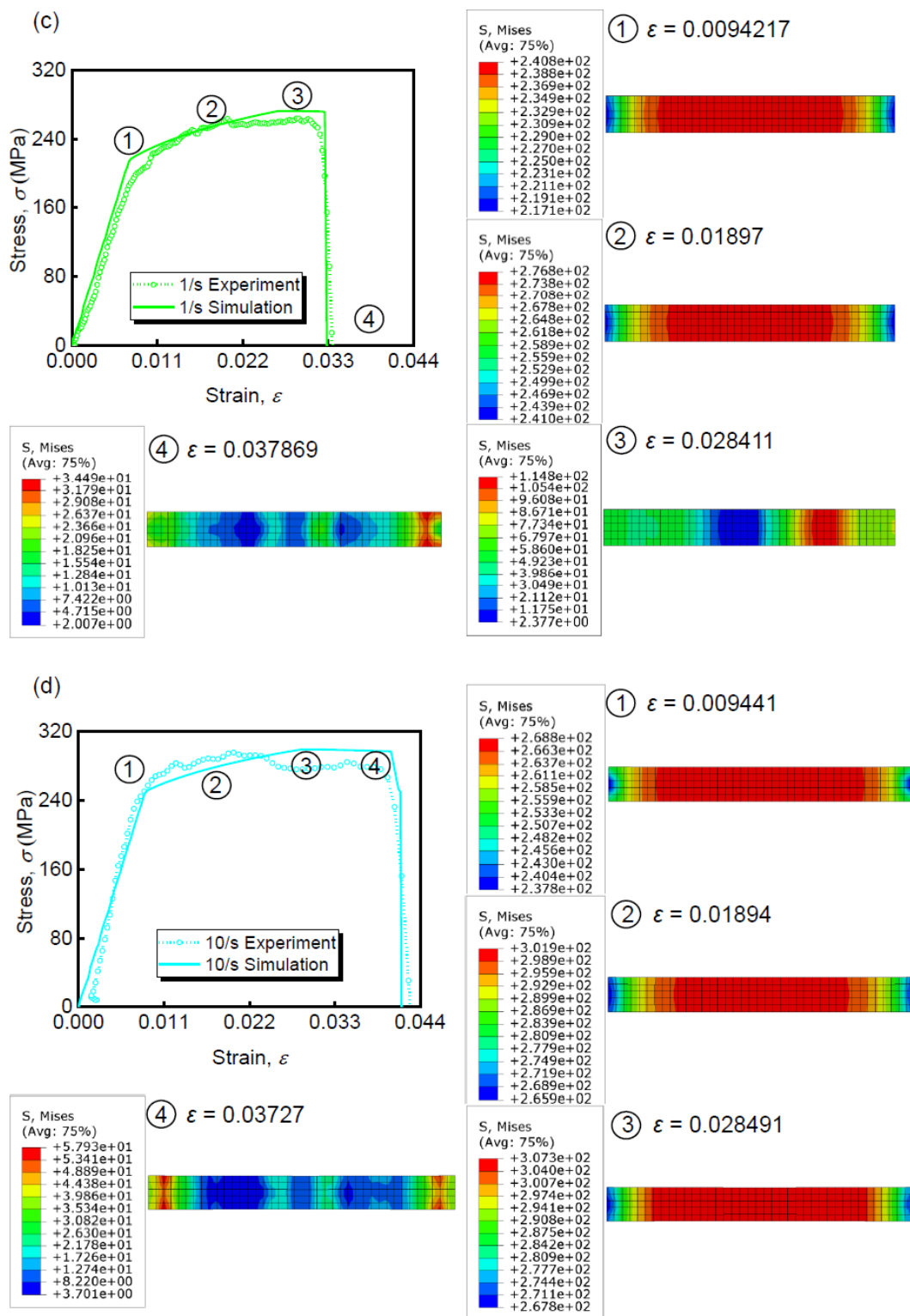


Figure 12: Stress vs strain comparison of anode current collector with simulation results showing contour plots at various instances from start of plastic stage to failure at SOC=0 along 0° for the following strain rates: (a) 0.01/s, (b) 0.1/s, (c) 1/s, (d) 10/s.

CHAPTER 4: RESULTS AND DISCUSSION

The following chapter focuses on the study of the results obtained from the experiment conducted with varying parameters as the angle of orientation of the samples, SOC, charging rate, charging/discharging cycles. The variable results obtained for the electrodes and the respective current collectors are compared along the parameters mentioned.

4.1. Anisotropic effect

The orientation of the sample at 0° , 45° , 90° , and the tensile testing experiment carried over each electrode, and respective current collectors were selected for the anisotropy effect study. Taking all the strain rates (i.e., 0.01/s, 0.1/s, 1/s, and 10/s) with respective loading velocities under consideration for this study, few variable parameters were fixed to receive an accurate result for the anisotropy. The fixed parameters were the SOC, charging rate, number of cycles as follows: SOC=0, 1-C charging rate, and 1 cycle of charging and discharging. To understand the behavior for electrode and current collector, it is needed to understand the orientation and direction of the samples being tested. In the experiment setup, the direction of sampling and details regarding how the electrode is cut out is mentioned and illustrated in Figure 7(c) and (d).

Each modulus calculated for the electrode and current collector has shown a minor change in the values with respect to the strain rates. For ease of understanding and comparison, a common modulus was selected for the complete electrode of a battery at a particular orientation and the current collectors as well. These calculated moduli are included in Table Figure 13, Figure 14, Figure 15, Figure 16, Figure 35, Figure 36, and Figure 37 shows the comparison of the strain rates for each electrode and respective current collectors for each orientation (i.e., 0° , 45° , and 90°). Referring these figures, it is observed the anode electrode in 45° orientation dominates as they have the

highest stress. Cathode electrode 0° has the largest modulus $E = 4819.42$ MPa, the 45° sample has the smallest $E = 3003.39$ MPa, and the 90° sample in between them with $E = 3994.85$ MPa. Since the orientation in 0° does not experience loading or rolling when they are rolled into the jellyroll during manufacturing, a higher young's modulus E is detected. Contradictory, the 90° orientation rolled during the manufacturing, is stronger than 45° orientation samples since they are semi-rolled, making them less flexible. The 0° orientation samples have the largest elastic modulus $E = 31364.87$ MPa, 90° orientation samples have the smallest modulus $E = 26408.21$ MPa, and 45° orientation sample have modulus $E = 27999$ MPa in between 0° and 90° samples for the cathode current collector which is an aluminum foil.

For the anode electrode, the 45° orientation samples have the largest modulus $E = 3719.46$ MPa followed by a 0° orientation sample with $E = 3327.66$ MPa and then lowest for 90° orientation with $E = 2718.84$ MPa. As the electrode is flattened out on the table during sampling, the active material and current collector get strongly bonded in at 45° orientation which results in the increased modulus as it is discovered. In the 0° orientation sample, due to rolling during the manufacturing of the jellyroll, the bond between the active material and current collector weakens; hence the flexibility of active material is lost when flattened. In the 90° orientation samples, the active material is most brittle than the other two orientations. These observations depict the variation occurring in the modulus E at different orientations. Similarly, for the anode current collector which is a copper foil, the modulus $E = 30912$ MPa is largest at 90° followed by 45° with $E = 29282.3$ MPa and smallest for 0° , i.e., $E = 20406.53$ MPa. The trend of moduli variation in anode current collector is opposite to that in cathode current collectors which proves the anisotropy behavior through the current collectors.

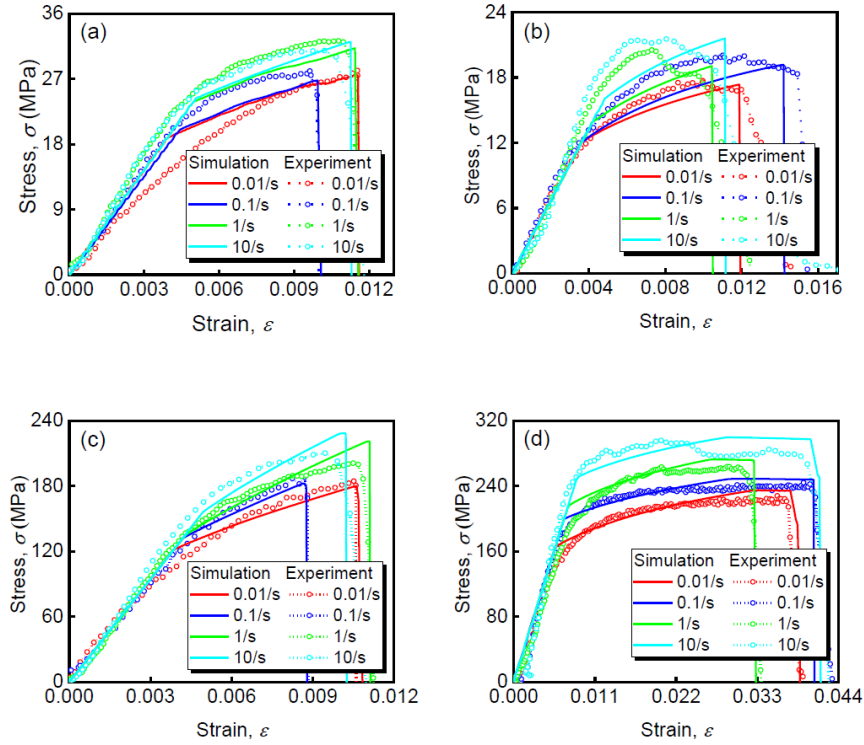


Figure 13: Stress vs strain comparison of experiment and simulation curves at 0.01/s, 0.1/s, 1/s, 10/s strain rates along 0° for: (a) cathode electrode with active material at SOC=0, (b) anode electrode with active material at SOC=0, (c) cathode current collector at SOC=0, (d) anode current collector at SOC=0.

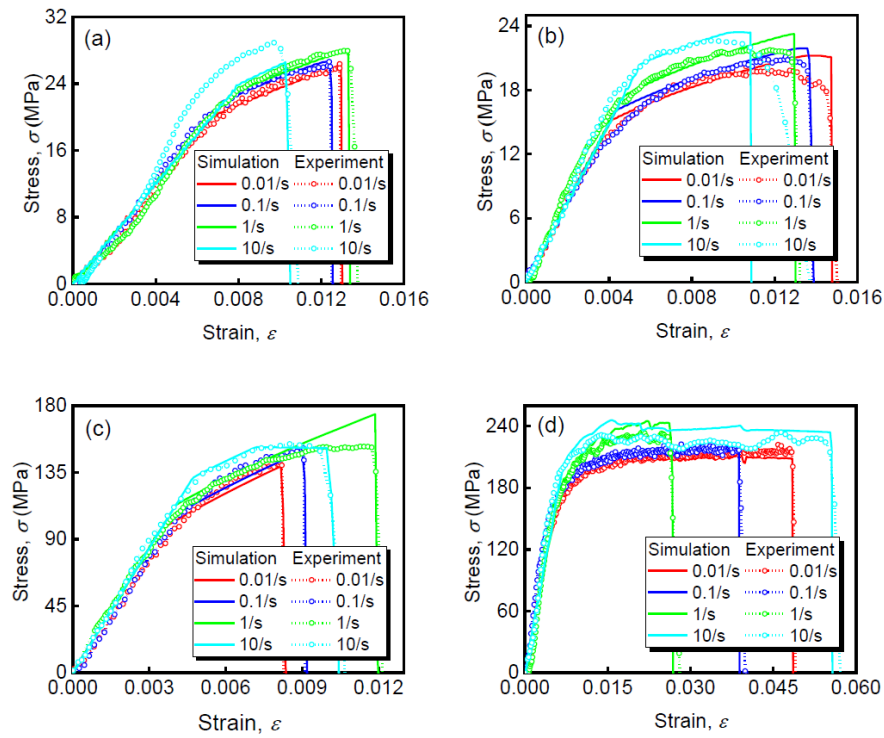


Figure 14: Stress vs strain comparison of experiment and simulation curves at 0.01/s, 0.1/s, 1/s, 10/s strain rates along 45° for: (a) cathode electrode with active material at SOC=0, (b) anode electrode with active material at SOC=0, (c) cathode current collector at SOC=0, (d) anode current collector at SOC=0.

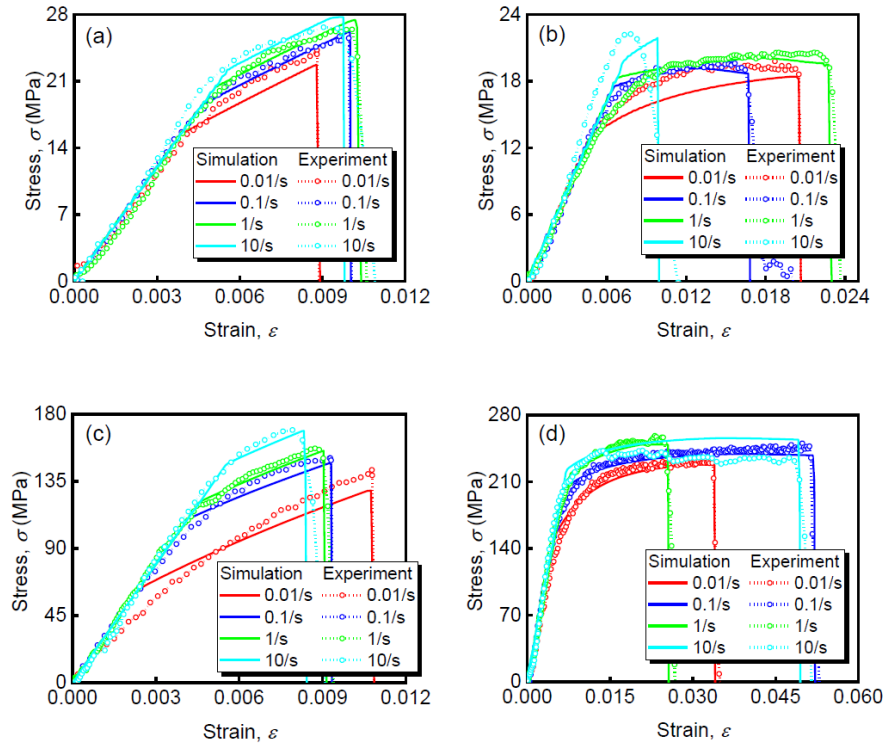


Figure 15: Stress vs strain comparison of experiment and simulation curves at 0.01/s, 0.1/s, 1/s, 10/s strain rates along 90° for: (a) cathode electrode with active material at SOC=0, (b) anode electrode with active material at SOC=0, (c) cathode current collector at SOC=0, (d) anode current collector at SOC=0.

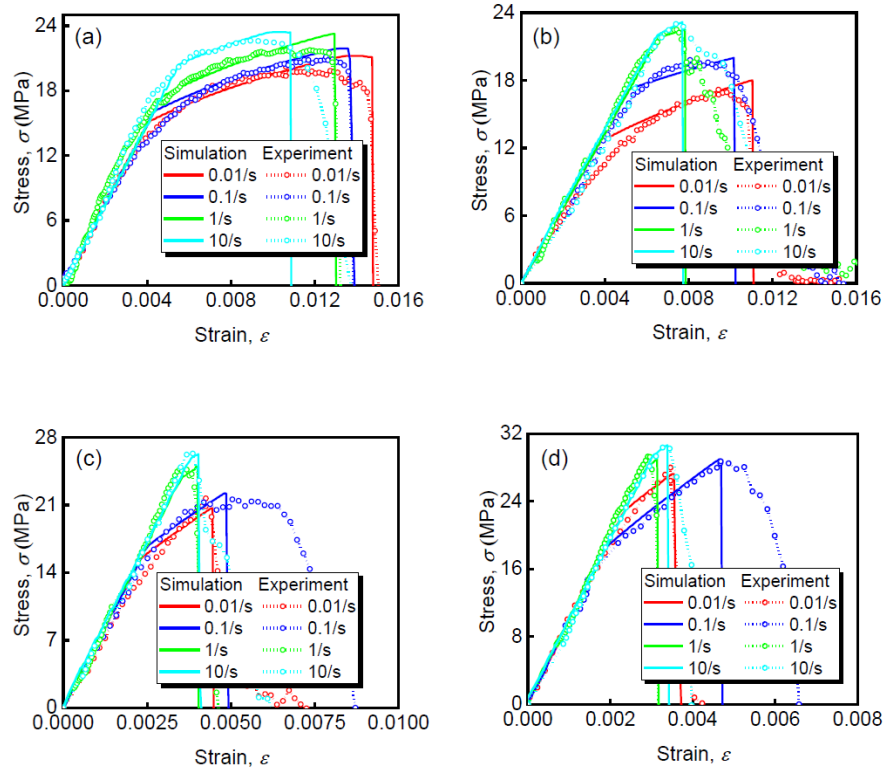


Figure 16: Stress vs strain comparison with different strain rates for anode electrode with active material samples for different SOC along 45° with simulation results: (a) SOC=0, (b) SOC=0.2, (c) SOC=0.4, (d) SOC=0.6.

4.2. Strain rate effect

The change in loading speed has a significant impact on the stress-strain curve plotted for the individual variable samples. Table 3 provides the yield stress σ_y and yield strain ε_y calculated for the anode, cathode, and respective current collector at 0° , 45° and 90° orientations, 1-C charging rate, 1 cycle, SOC=0, and at all the strain rates (i.e., 0.01/s, 0.1/s, 1/s, and 10/s). The yield stresses σ_y show an increment in the values with increasing the strain rates which supports the strain rate effect claim. Even with the increment in the stress, there is no considerable effect on the yield strains ε_y of these samples. Since the manufacturing of the electrode, a number of parameters are considered which affect the yield strain behavior. A minor change is observed due to variation or damage during electrode fabrication.

All the curves plotted with the variable parameters, i.e., the orientations (0° , 45° , 90°), the charging rates (0.1-C, 0.5-C, 1-C, 2-C), number of cycles (1 cycle, 10 cycles, 50 cycles, 100 cycles), SOCs (0, 0.2, 0.4, 0.6) show the strain rate effect throughout. Figure 13 (a)-(d), Figure 14(a)-(d), Figure 15(a)-(d), Figure 16(a)-(d) show the stress -strain curves for the four strain rates at the four respective loading velocities exerting the strain rate effect as mentioned above.

The possible cause of the electrodes, i.e., anode and cathode, along with the respective current collectors to exhibit this behavior can be stated due to the homogeneous isotropic behavior of active materials and the current collectors. An increase in the loading speed increases the strength of the material to resist; hence we observed increased stress curves. This phenomenon of increase in strength is common in electrodes and current collectors even with isotropy and anisotropy behavior in the materials. Working on the numerical simulations for the experiment for different

orientations, the strain rate effect was governed by Johnson-Cook model. From Eq. (2) it can be seen the modified Johnson-Cook equation has the dimensionless quantity ($\frac{\epsilon_{pl}}{\epsilon_0}$) which used the strain rate used in the experiment to define the plastic stage behavior in the numerical simulation hence governing the strain rate effect. Figure 13(a)-(d), Figure 14(a)-(d), Figure 15(a)-(d), and Figure 16(a)-(d) impart a convincing justification of the strain rate coupling phenomenon induced due to mechanical behavior with the agreement of the experimental and numerical simulation curves.

4.3. SOC effect

For the study of the SOC effect, the parameters (orientation, charging rate, number of cycles) except the SOC of the battery were fixed. Fixing these parameters helps in investigating the behavior of the battery for different SOC. The parameters fixed for this investigation are as follows: orientation is 45° , Charging rate is 1-C, number of charging/discharging cycles=1. The SOC is nothing but an amount of charging the battery has after charging. In this thesis study, the battery at SOC=0, SOC=0.2, SOC=0.4, and SOC=0.6 that is the batteries are at complete discharge, 20% charging, 40% charging, and 60% charging. All the parameters with variable SOC are compared for the different strain rates mentioned (i.e., 0.01/s, 0.1/s, 1/s, and 10/s). Working with SOC is a crucial job, a minor mistake can lead to internal short-circuiting or damage to the battery. SOC beyond 0.5, i.e., 50% charging, is very hazardous and difficult to work. It is a work of delicacy and utmost caution. Working on the mentioned SOC has provided enough data during the tensile test that could be used for studying this effect in 21700 LIBs.

Curves from Figure 17 (a)-(d) illustrate the comparison of anode electrode in 45° orientation for SOC=0, 0.2, 0.4 and 0.6. The material/anode active material is seen to

become stiffer with the SOC. As the SOC increases, the thickness of the anode electrode increases due to the transfer of lithium ions in the anode hence swelling the anode active material. The stiffness of any material is dependent on the thickness of that material sample. Working on the experiment, the thickness of each sample was measured, as mentioned in the experiment section. It was observed there was a significant increase in the thickness of anode samples. This study supports the claim of increasing stiffness with an increase in the SOC; hence we can see the rise in stress-strain curves. The increasing SOC facilitates an increase in volume up to 6.18 % from SOC=0 to SOC=0.6 for anode active material which is graphite. This volume expansion is a result of the transfer of Li-ions of lithiation. Another effect on the battery electrode with an increase in SOC was that the material became brittle and hence the failure strain ϵ_f of this electrode reduces. Figure 17(e)-(h) is the comparison of the anode current collector with respect to increasing SOC. Even with the increase in SOC, the stress-strain curves for all the samples with the current collector for mentioned SOC's of 0, 0.2, 0.4, and 0.6 have nearly the same curve that states the mechanical behavior of these pure anode current collector is independent of the SOC.

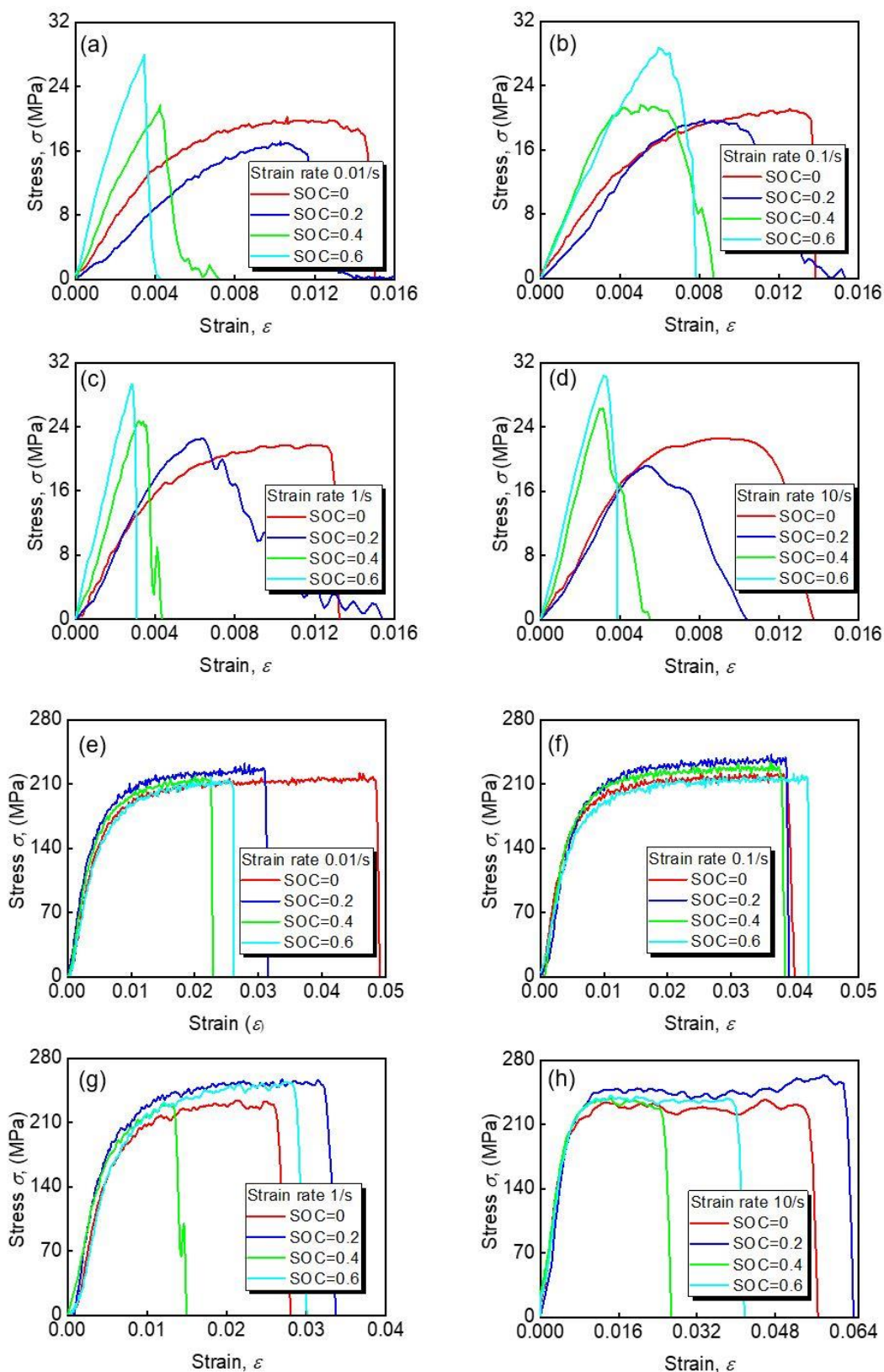


Figure 17: Stress vs strain curves for anode electrode with active material samples comparing different SOC (i.e. 0, 0.2, 0.4 and 0.6) along 45° for strain rate of: (a) 0.01/s, (b) 0.1/s, (c) 1/s, (d) 10/s, for anode current collector samples comparing different SOC (i.e. 0, 0.2, 0.4 and 0.6) along 45° for strain rate of: (e) 0.01/s, (f) 0.1/s, (g) 1/s, (h) 10/s.

Figure 18(a)-(d) and Figure 18(e)-(h) show the curves for various strain rates compared to the cathode electrode and its current collector, respectively. The cathode electrode's stress-strain curves drop with an increase in SOC. Due to lithiation and de-lithiation, the transfer of ions aids in the decrement of the cathode electrode. Thus, at SOC=0, we have the strongest stress-strain curve, and at SOC=0.6, we have the weakest. Equivalent to the anode and its current collector, the decrease in failure strain ϵ_f with incremental SOC is noticed in the cathode and its current collector as well. Per lithiation and de-lithiation, Li-ions move from cathode to anode. The thickness of the cathode decreases up to 5 μm , which causes a volume reduction of 2.98% from SOC=0 to SOC=0.6. In the manner of the cathode electrode, the cathode current collector also inherits a similar trend. Differentiating from the anode current collector, the cathode current collector is dependent on the SOC. A previous literature study has investigated and proved the change in material properties is a reaction that is carried out in the active materials of the electrode. Yet still, the cathode current collector here for 21700 LIB shows a similar as to the cathode electrode. SOC increment facilitated the corrosion in the current collector. Anode current collector resists better than the cathode current collector which results in degrading battery performance. The binding of the active materials and current collectors is the key to this phenomenon. Cathode electrode being denser than anode electrode binding of cathode active material with its current collector (i.e. aluminum foil) is stronger as compared to that of the anode electrode and its current collector (i.e. copper foil), making cathode more vulnerable as deposition of Li-ions over the current collector facilitates the corrosion. [68, 82, 83]. The cathode current collector gets porous with these increasing SOC, and hence even with no change in the cathode current collector's thickness, a decremental trend in the stress-strain curves is observed.

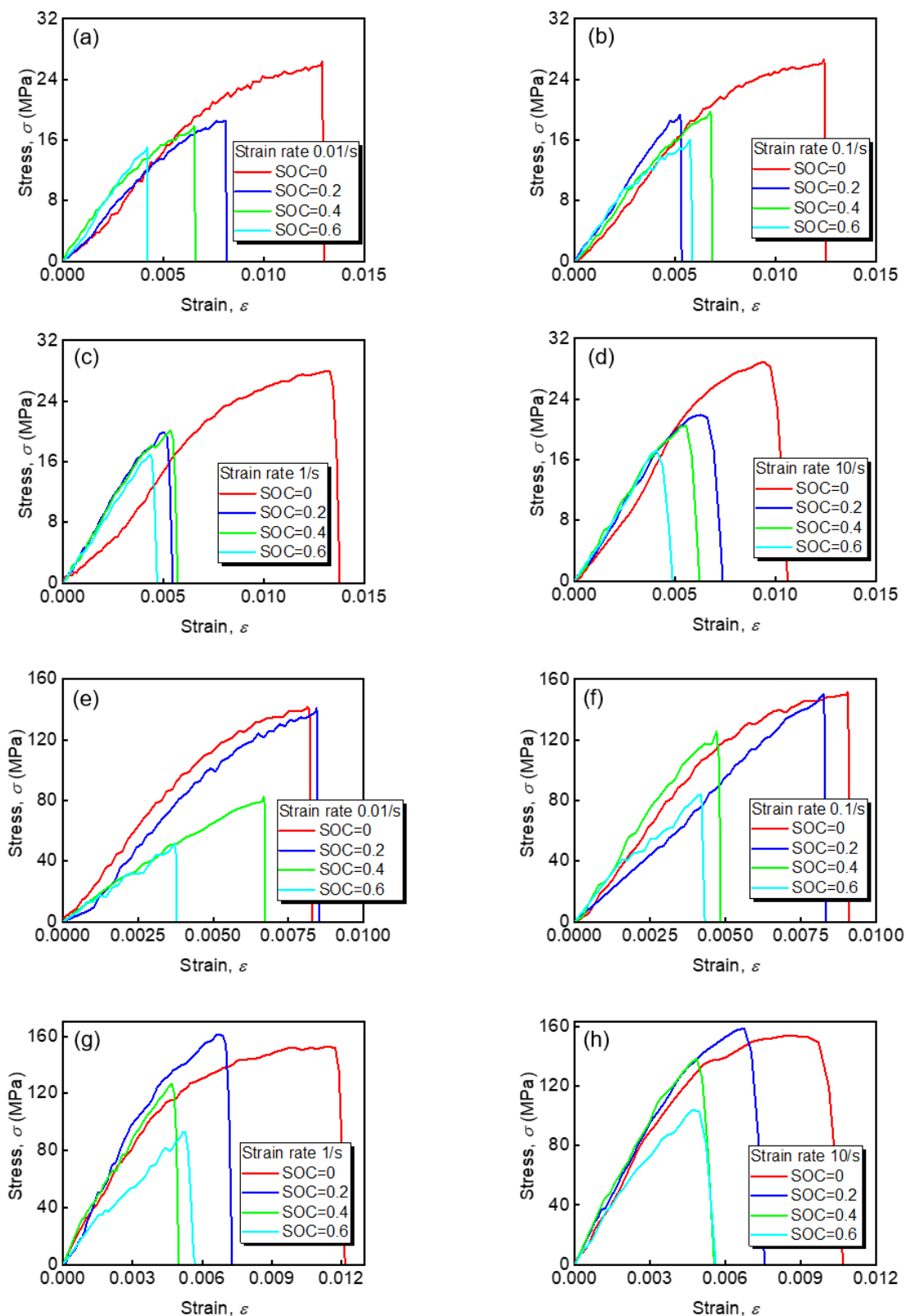


Figure 18: Stress vs strain curves for cathode electrode with active material samples comparing different SOC (i.e. 0, 0.2, 0.4 and 0.6) along 45° for strain rate of: (a) 0.01/s, (b) 0.1/s, (c) 1/s, (d) 10/s, for cathode current collector samples comparing different SOC (i.e. 0, 0.2, 0.4 and 0.6) along 45° for strain rate of: (e) 0.01/s, (f) 0.1/s, (g) 1/s, (h) 10/s.

4.4. Charging rate effect

The study of the charging rate is induced to understand the behavior of the 21700 LIB. Charging rate behavior in LIBs are in a recent study for lithium plating behavior. For the 21700 LIB the investigation of anode, cathode, and respective current collectors for different charging rates can lead to the development of the manufacturing of better battery models to be used commercially. This study investigates the mechanical behavior of each sample under tensile testing. The charging rate used in the study is 0.1-C, 0.5-C, 1-C, and 2-C. These charging rates are compared for different strain rates. The sample parameters used for this effect study is 0° orientation, at SOC=0, and at all the four strain rates. The comparison is provided separately for each strain rate.

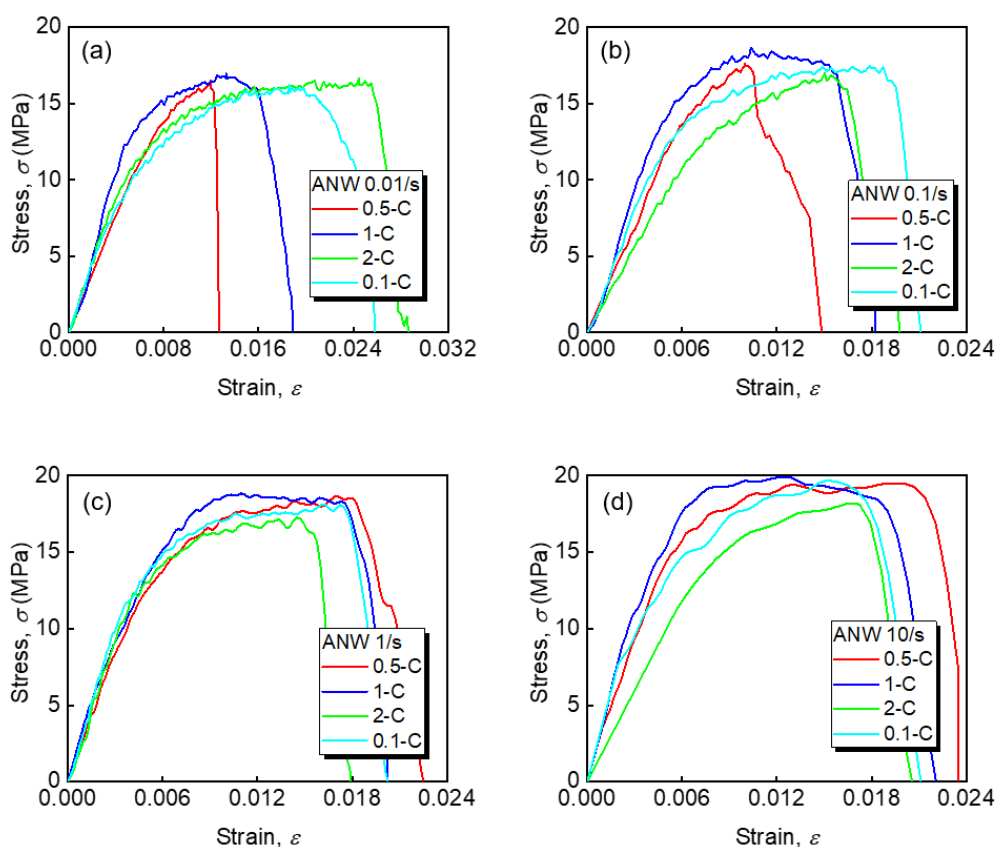


Figure 19: Stress vs strain experiment curves for anode electrode with active material comparing charging rates 0.1-C, 0.5-C, 1-C and 2-C at 1-cycle, SOC=0 for 0° samples.

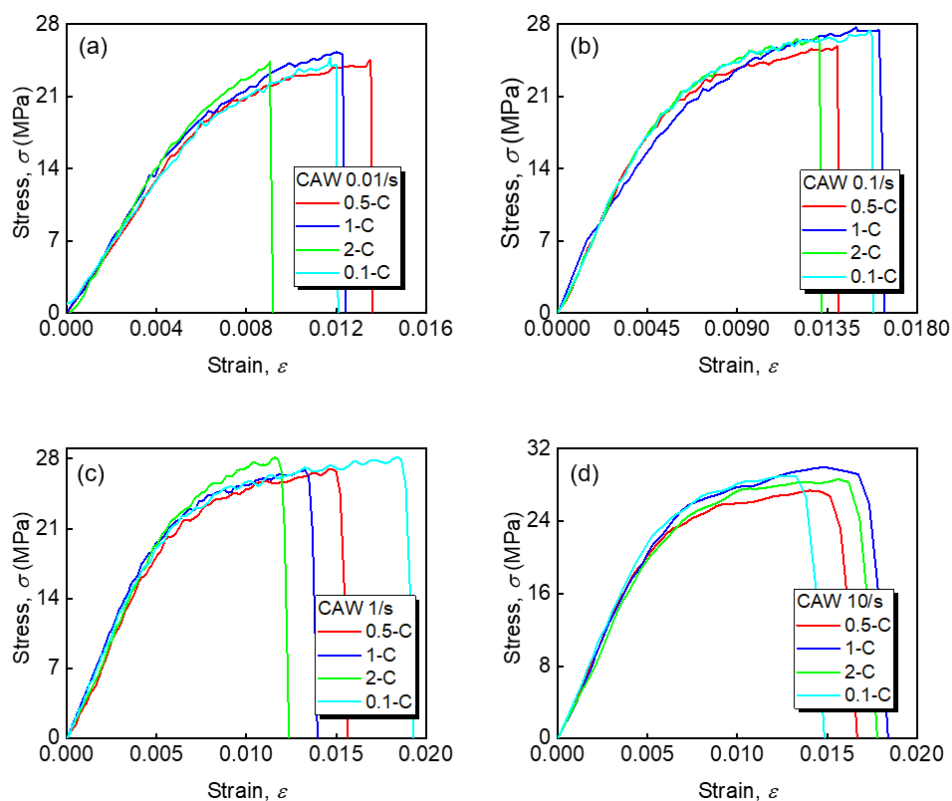


Figure 20: Stress vs strain experiment curves for cathode electrode with active material comparing charging rates 0.1-C, 0.5-C, 1-C and 2-C at 1-cycle, SOC=0 for 0° samples.

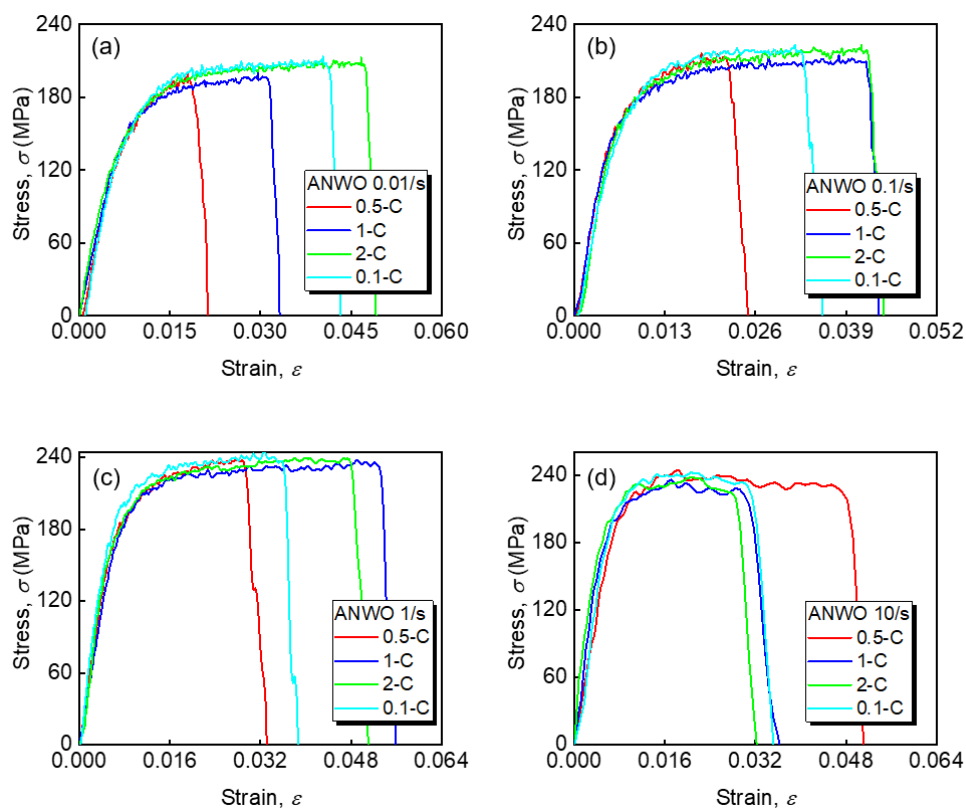


Figure 21: Stress vs strain experiment curves for anode current collector comparing charging rates 0.1-C, 0.5-C, 1-C and 2-C at 1-cycle, SOC=0 for 0° samples.

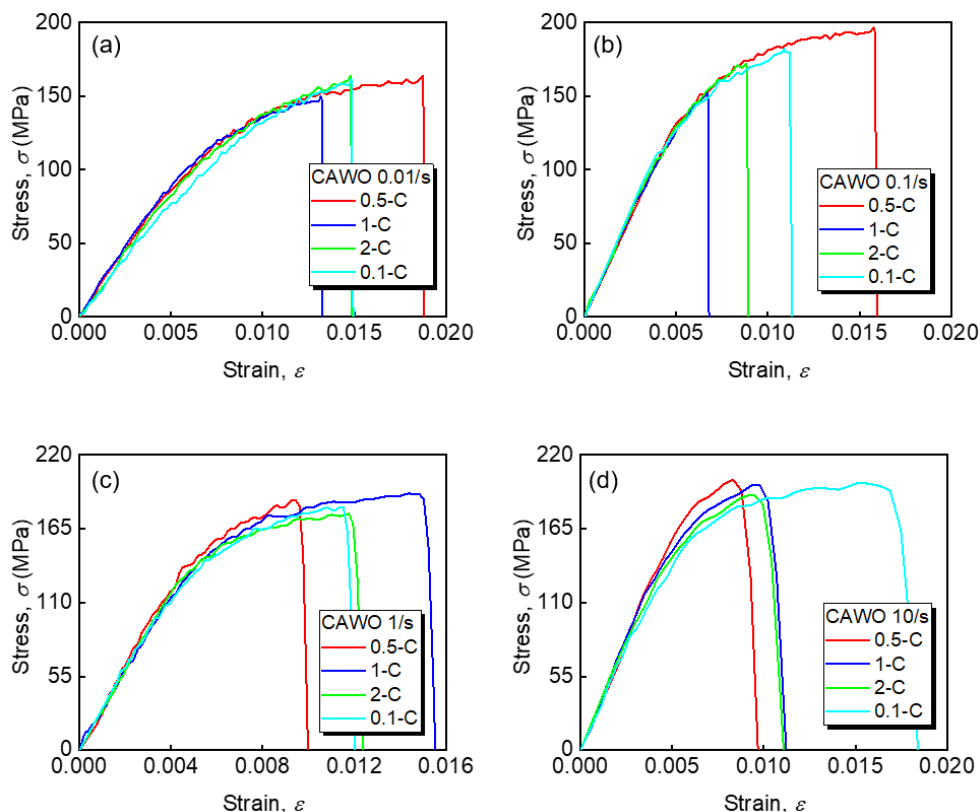


Figure 22: Stress vs strain experiment curves for cathode current collector comparing charging rates 0.1-C, 0.5-C, 1-C and 2-C at 1-cycle, SOC=0 for 0° samples.

Figure 19(a)-(d), Figure 20(a)-(d), Figure 21(a)-(d), and Figure 22(a)-(d) shows the comparison of different charging rate for 1- cycle battery electrodes and respective current collectors at individual strain rates. The anode electrode curves for the charging rates have a trend in which 1-C battery has the highest stress carrying capacity, followed by 0.5-C and then 0.1-C. A similar trend of charging rates is observed for all the strain rates (i.e., 0.01/s, 0.1/s, 1/s, and 10/s). At lower strain rates, the 2-C and 0.1-C charging rate curves are nearly the same. The difference in the strain curves at various charging rate is nearly 0.4-0.5 MPa. Cathode electrode, on the other hand, has no effect due to the charging rates 2-C, 1-C, and 0.1-C. 0.5-C charging rate curve is lower than the other charging rate curves. The charging rate has a slight impact on the mechanical behavior as noticed the charging rate at 2-C makes the battery soft and brittle making it drop the stress curve. A similar trend for 0.5-C charging but with a lower stress curve. Figure 20(a)-(d) shows the cathode curves comparing charging rates for each strain rate. There

is no significant change in the mechanical behavior of the cathode electrode for any of the strain rates.

Figure 21(a)-(d) and Figure 22(a)-(d) show the comparison curves for anode current collector and cathode current collector. Even with the change in the charging rate, there is no change in the curves for any of the strain rates. This states the current collectors are independent of the charging rates.

At lower cycling of the batteries does not have any significant change in the charging rate since the electrodes do not get significantly erode. With increasing cycling of the battery, the lithium-ion exchange leads to the weakening of active materials hence lower strength and stiffness of the electrodes.

As the cycling of the battery increases to 50 cycles and 100 cycles, the cathode electrode, anode current collector, and the cathode current collector have no change in the stress-strain plots. Figure 27(a)-(d), Figure 28(a)-(d), Figure 29(a)-(d), Figure 30(a)-(d), Figure 31(a)-(d), Figure 32(a)-(d), Figure 33(a)-(d), and Figure 34(a)-(d) provides proofing to the statement above. Cathode being the electrode does not get affected as it is a denser material and has a stronger bonding with the current collector, following up from the previous discussion on SOC effect. For the anode electrode, however, the curves with 0.5-C charging rate have a higher curve stating stiffer and stronger materials. 0.5-C curves are followed by 2-C and then 1-C in the stress-strain plots. For lower strain rates at 0.01/s and 0.1/s the strength of the electrodes is nearly the same; hence a similar curve pattern emerges. Due to the lower loading speed, the material is under quasi-static loading which results in a similar trend of plots observed.

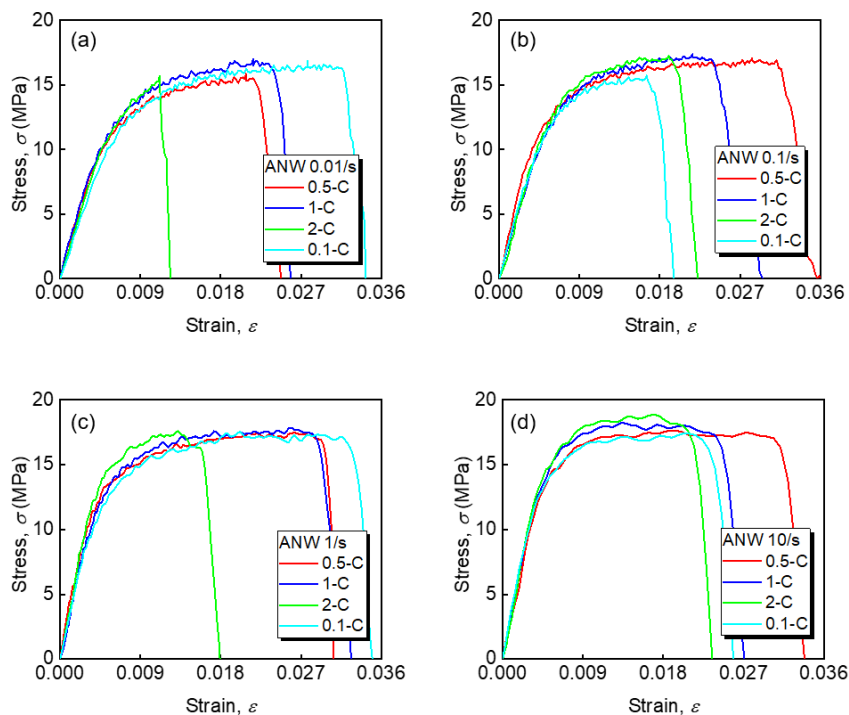


Figure 23: Stress vs strain experiment curves for anode electrode with active material comparing charging rates 0.1-C, 0.5-C, 1-C and 2-C at 10-cycle, SOC=0 for 0° samples.

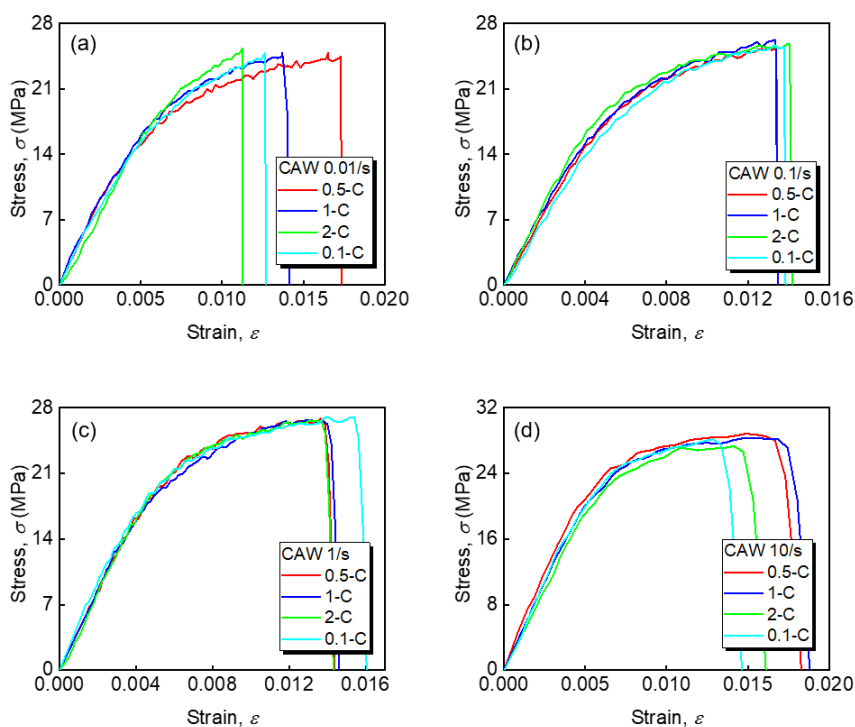


Figure 24: Stress vs strain experiment curves for cathode electrode with active material comparing charging rates 0.1-C, 0.5-C, 1-C and 2-C at 10-cycle, SOC=0 for 0° samples.

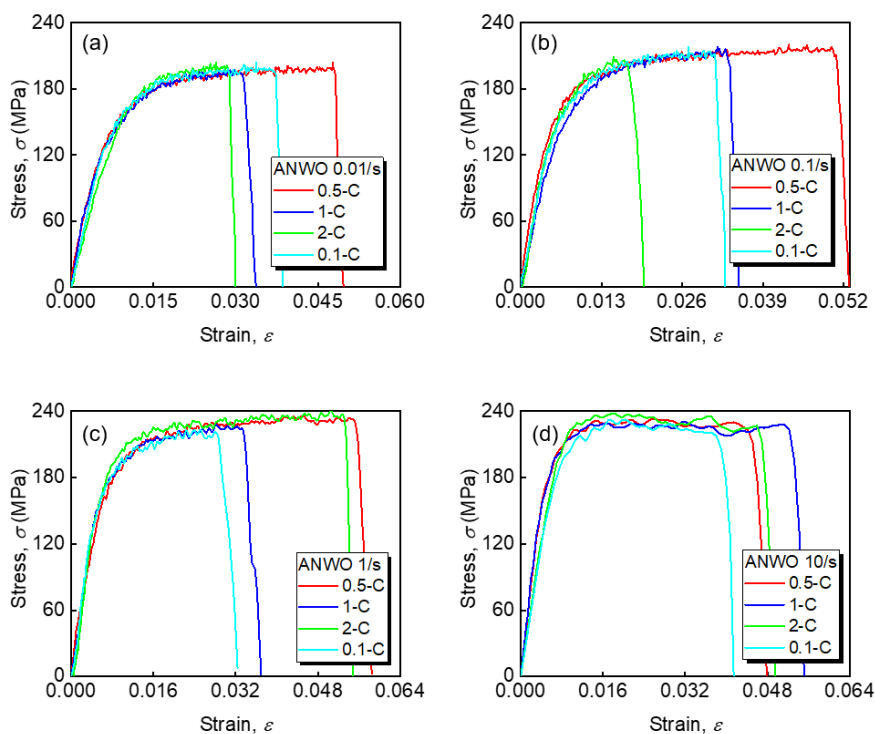


Figure 25: Stress vs strain experiment curves for anode current collector comparing charging rates 0.1-C, 0.5-C, 1-C and 2-C at 10-cycle, SOC=0 for 0° samples.

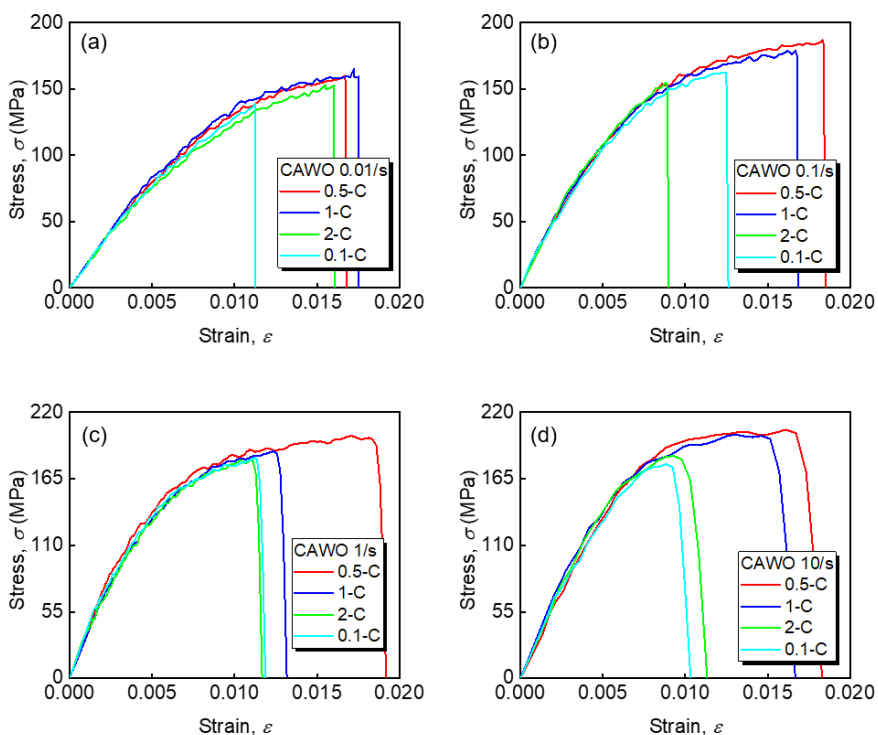


Figure 26: Stress vs strain experiment curves for cathode current collector comparing charging rates 0.1-C, 0.5-C, 1-C and 2-C at 10-cycle, SOC=0 for 0° samples.

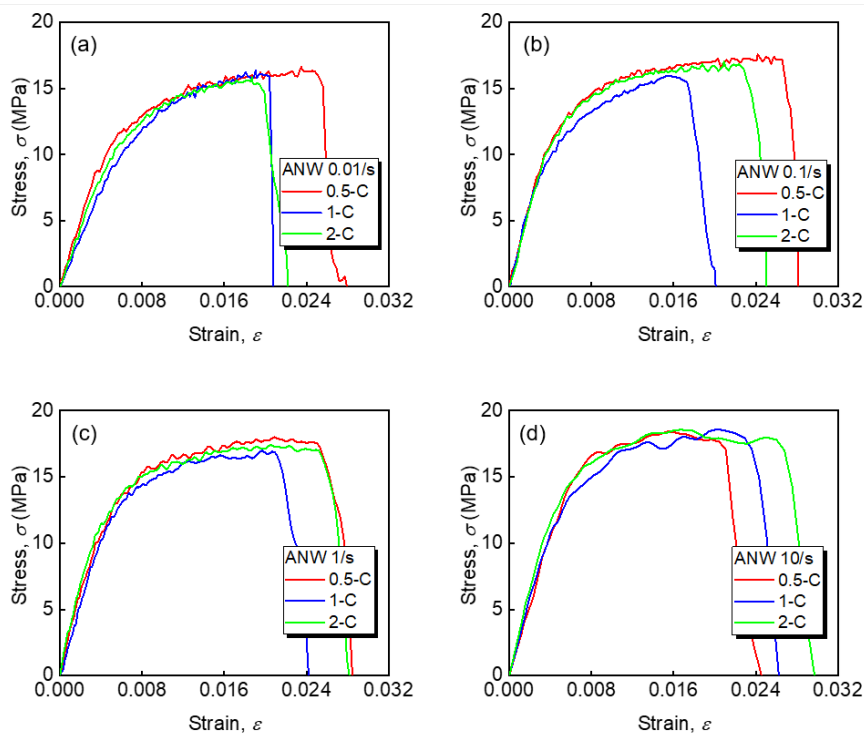


Figure 27: Stress vs strain experiment curves for anode electrode with active material comparing charging rates 0.5-C, 1-C and 2-C at 50-cycle, SOC=0 for 0° samples.

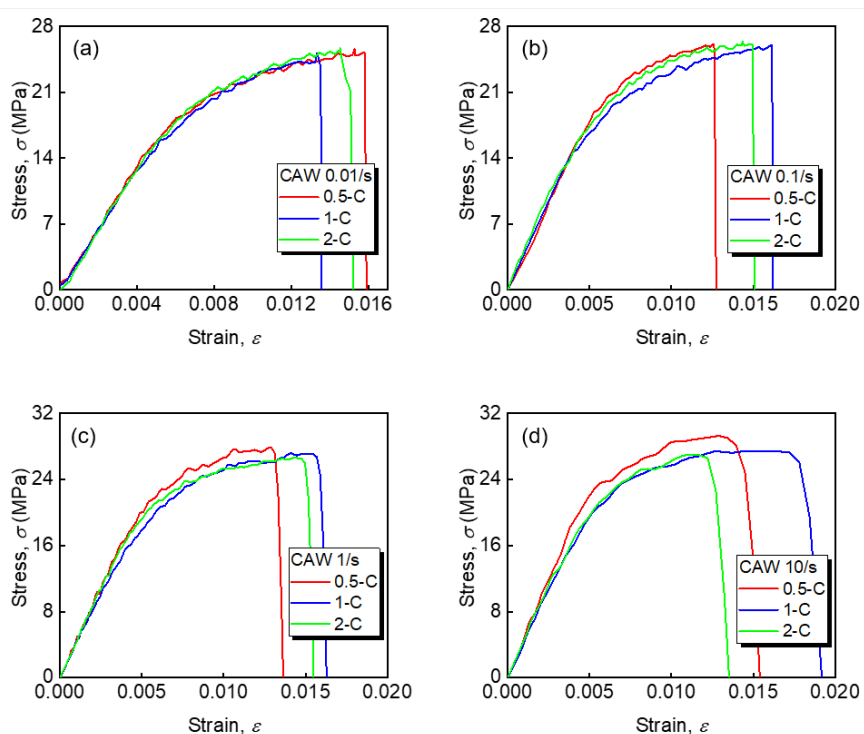


Figure 28: Stress vs strain experiment curves for cathode electrode with active material comparing charging rates 0.5-C, 1-C and 2-C at 50-cycle, SOC=0 for 0° samples.

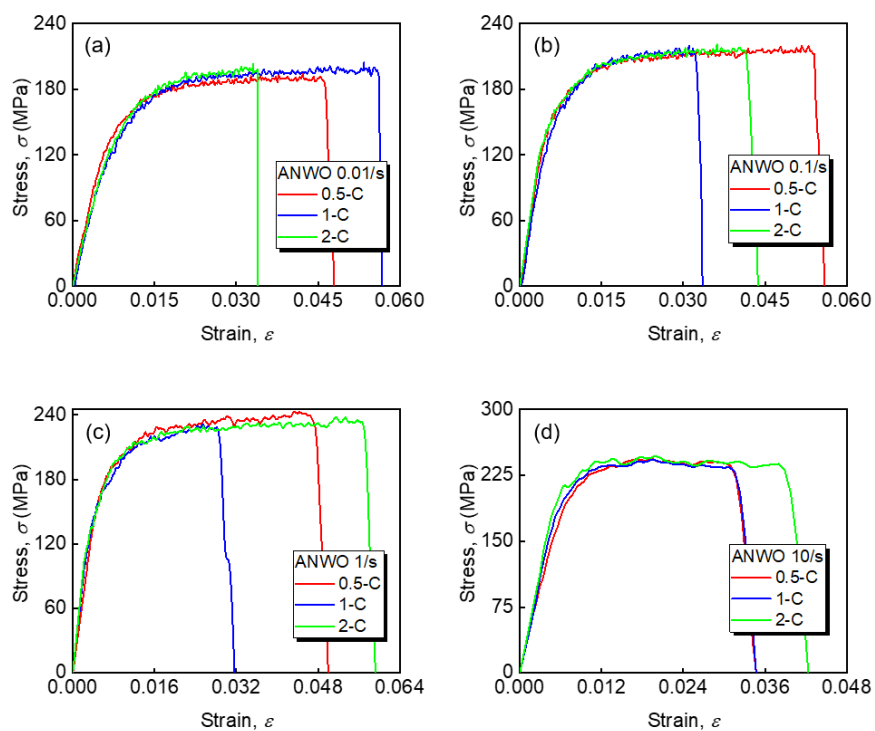


Figure 29: Stress vs strain experiment curves for anode current collector comparing charging rates 0.5-C, 1-C and 2-C at 50-cycle, SOC=0 for 0° samples.

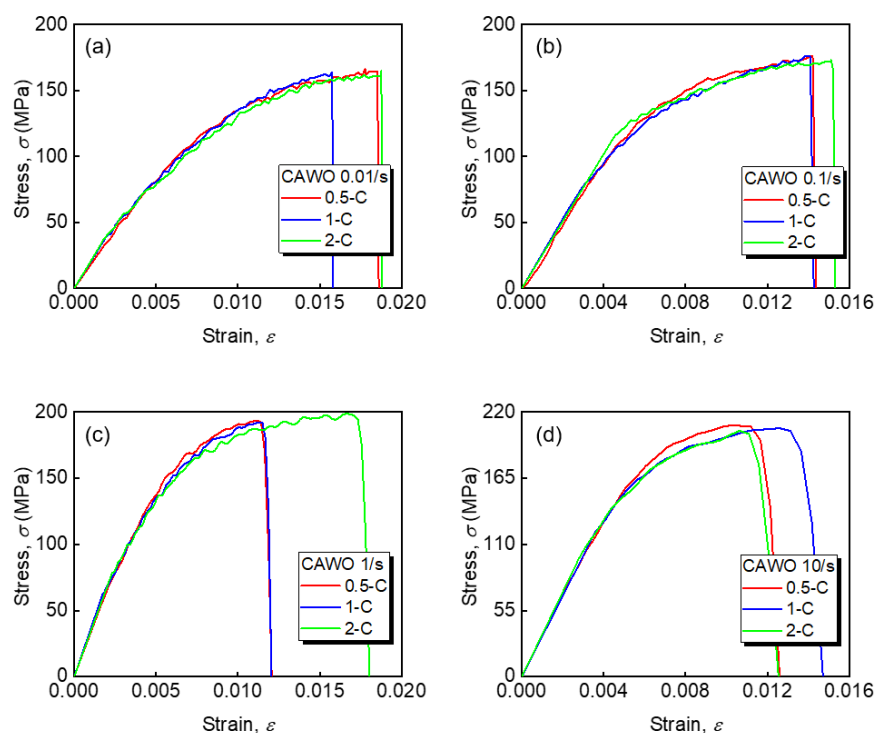


Figure 30: Stress vs strain experiment curves for cathode current collector comparing charging rates 0.5-C, 1-C and 2-C at 50-cycle, SOC=0 for 0° samples.

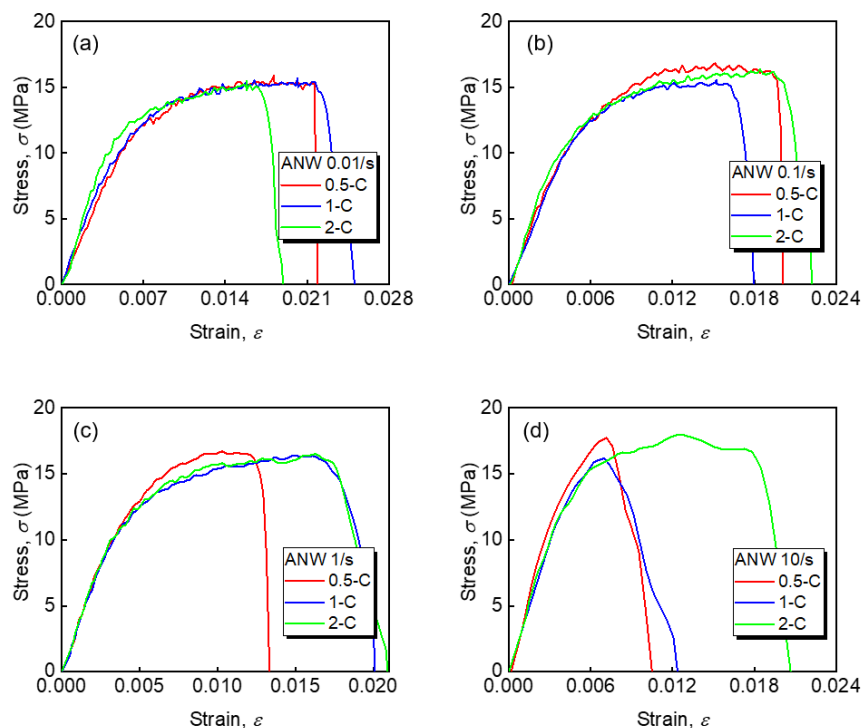


Figure 31: Stress vs strain experiment curves for anode electrode with active material comparing charging rates 0.5-C, 1-C and 2-C at 100-cycle, SOC=0 for 0° samples.

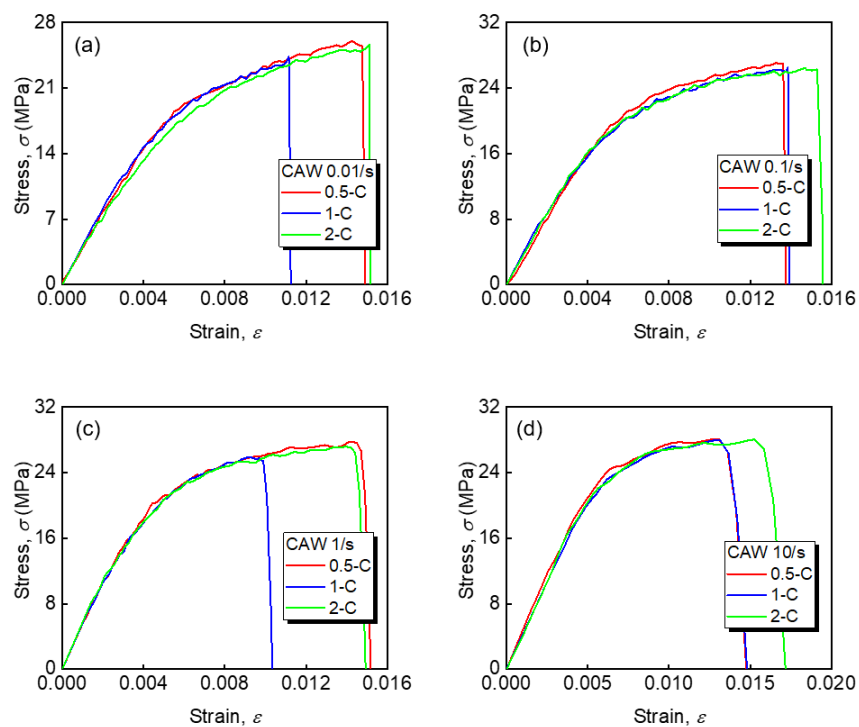


Figure 32: Stress vs strain experiment curves for cathode electrode with active material comparing charging rates 0.5-C, 1-C and 2-C at 100-cycle, SOC=0 for 0° samples.

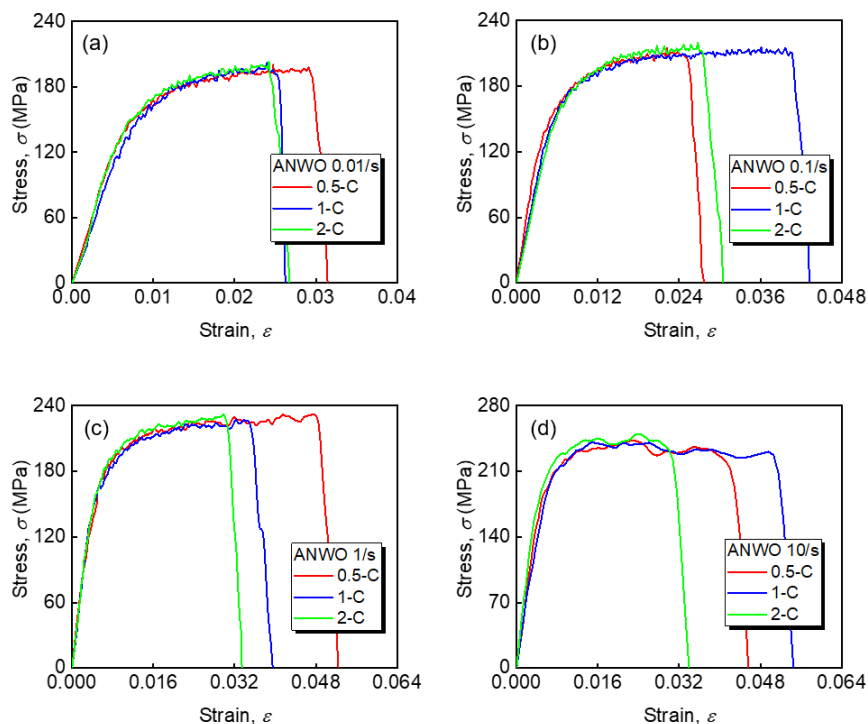


Figure 33: Stress vs strain experiment curves for anode current collector comparing charging rates 0.5-C, 1-C and 2-C at 100-cycle, SOC=0 for 0° samples.

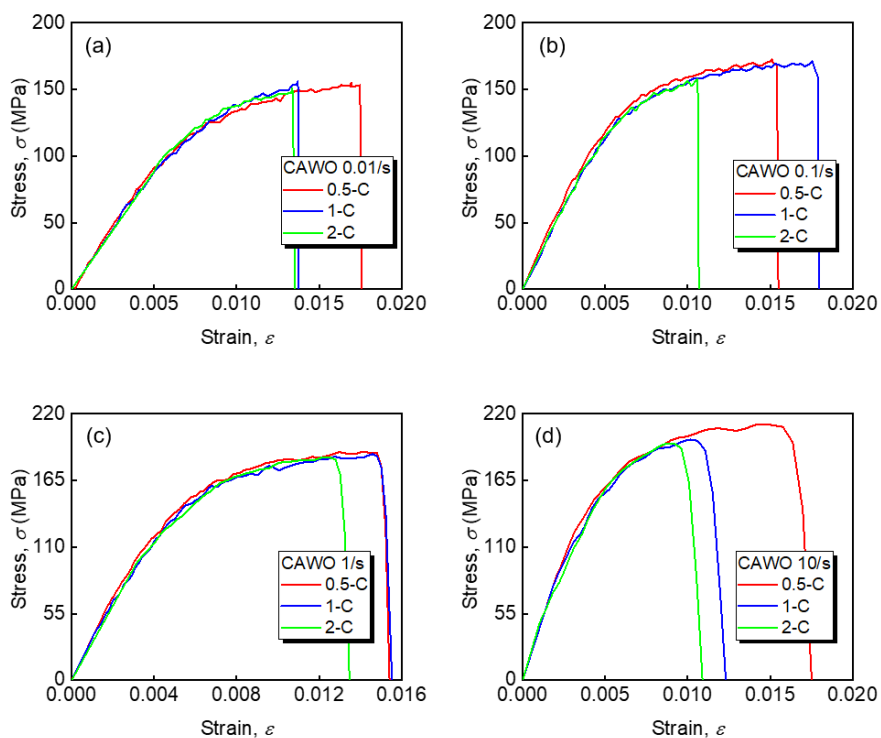


Figure 34: Stress vs strain experiment curves for cathode current collector comparing charging rates 0.5-C, 1-C and 2-C at 100-cycle, SOC=0 for 0° samples.

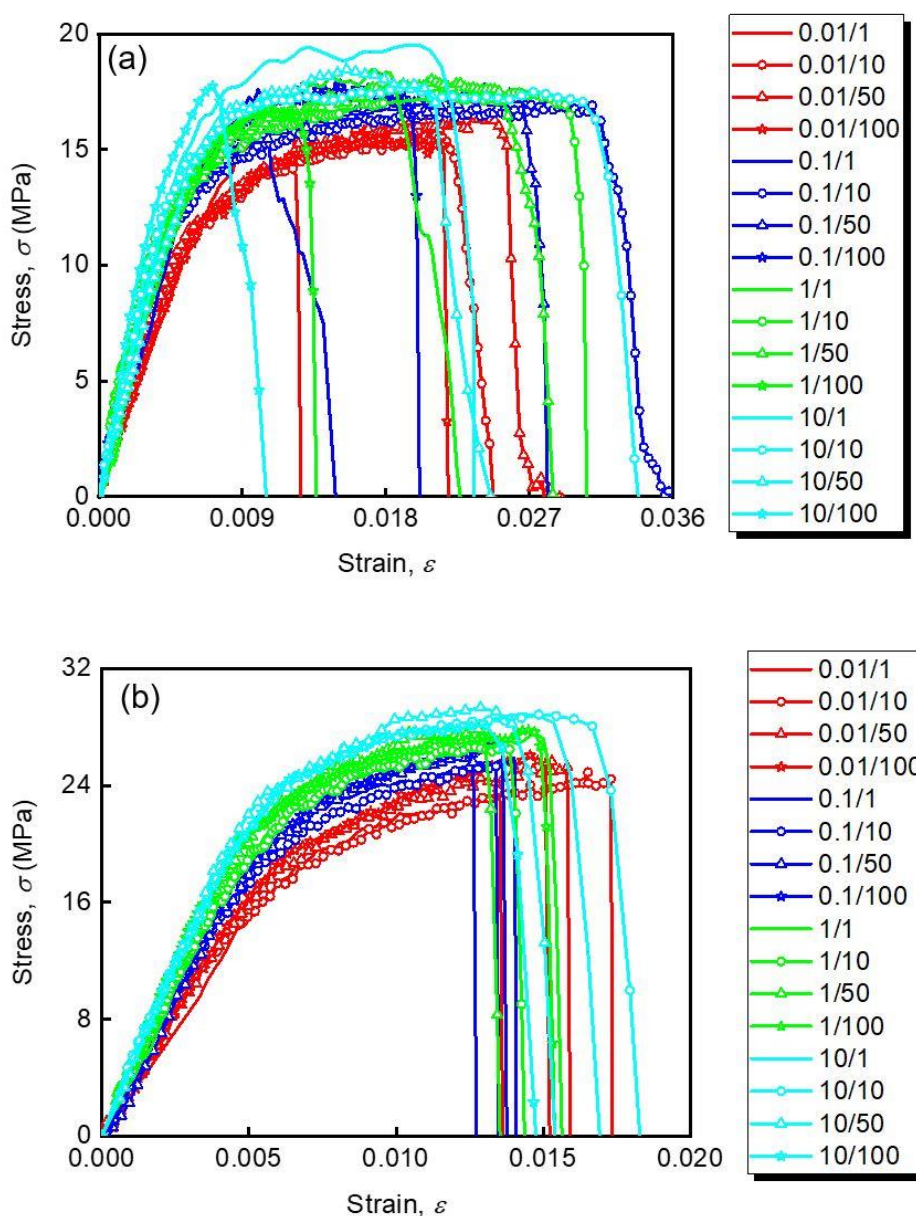
4.5. Cycling effect

The following sub-chapter provides a detailed analysis of the cycling effect with results succeeding the tensile testing of the electrodes and the respective current collector. Identical to the previous swotting of the effect, the parameters are fixed to get a clear picture and understanding of the effect. SOC=0, sample orientation at 0° , is fixed throughout. Charging rates of 0.5-C, 1-C, and 2-C are fixed separately to extract data comparing the parameters for 1 - cycle, 10 – cycles, 50 – cycles, and 100 cycles, respectively. Each of the strain rates (i.e., 0.01/s, 0.1/s, 1/s, and 10/s) are considered to investigate any change in the mechanical properties with respect to the change in the loading speed.

As previously indicated, the charging rates (0.1-C, 0.5-C, 1-C, and 2-C) have different behavior and mechanical response under tensile loading. Comparison of the same for all the cycles had provided with significant information stating as the cycles increase, meaning as the battery goes on aging, and it loses the performance. The electrodes fail to perform the task efficiently and hence leading to the deterioration of the electrodes. As mention in literature [78] battery fails to perform the lithiation and de-lithiation and hence starts leaking the electrolyte and may damage the whole battery pack and even the system which relies in the battery power.

Figure 35(a)-(d) shows the comparison of stress-strain curves for the strain rates and at 0.5-C charging rate. Additionally, comparisons for 1-C and 2-C charging rates are made in Figure 36(a)-(d) and Figure 37(a)-(d), respectively. From the previous discussion of strain rates, each electrode and current collector has a satisfactory strain rate effect, which can also be seen for the mentioned conditions. For each of the charging rates as the charging/discharging of the battery is increased, the curve for the anode electrode drop stating the diminution of the battery. The change in curves is

minor at lower strain rates, but it is distinguishable at higher strain rates. Cathode electrode as well gets weak and has a slight drop in the strength and stiffness as the number of cycles increase. Anode-cathode both shows the minor change in values which is hardly differentiated. On the contrary, the current collectors (both anode and cathode) are independent of the cycling rate. Even with a negligible trace of corrosion in the current collector at higher cycles, they show mechanical behavior independent to the number of cycles.



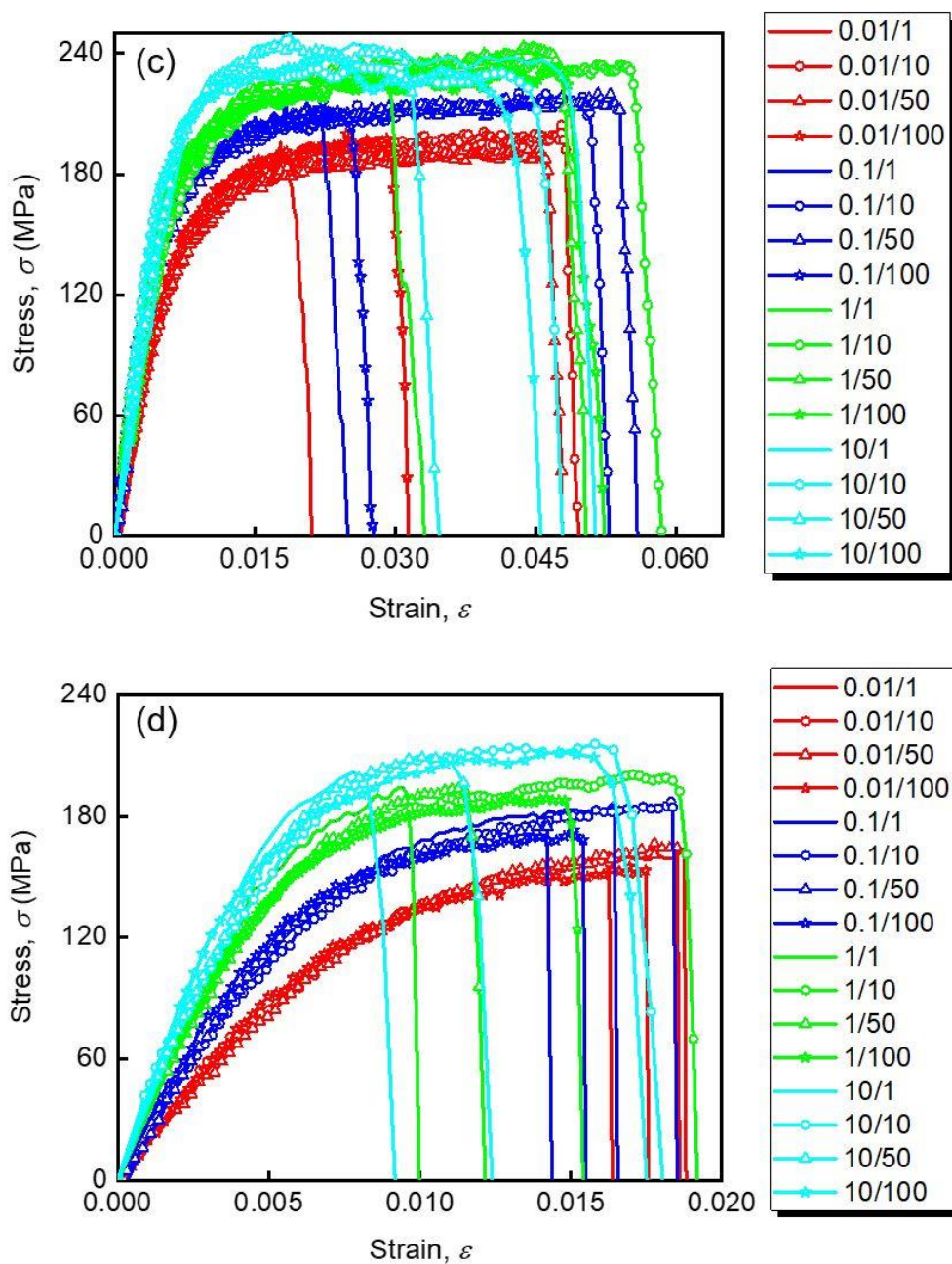


Figure 35: Stress vs strain curve comparing number of cycles at 0.5-C, SOC=0, 0° for (a) anode electrode with active material, (b) cathode electrode with active material, (c) anode current collector, (d) cathode current collector.

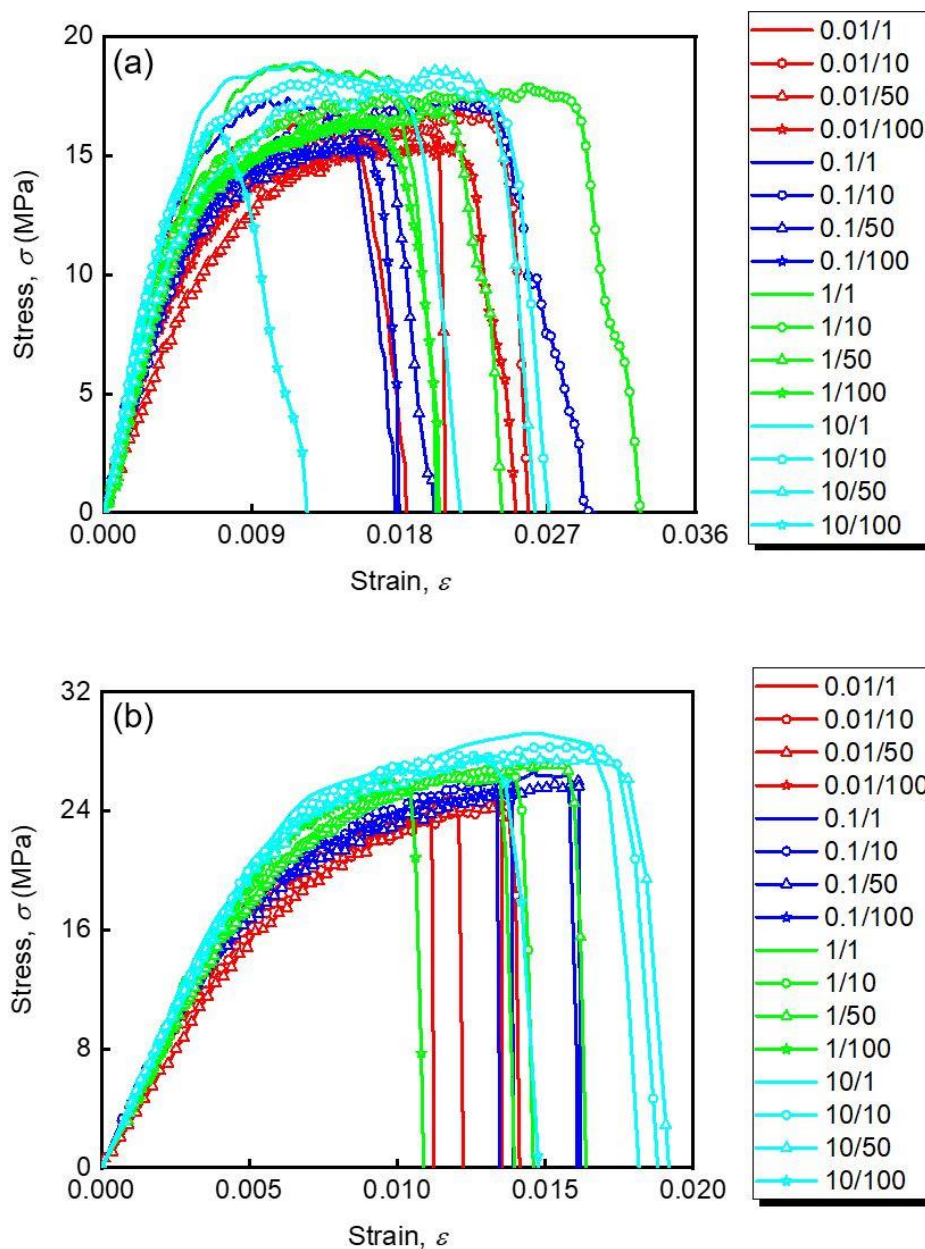


Figure 36: Stress vs strain curve comparing number of cycles at 1-C, SOC=0, 0° for (a) anode electrode with active material, (b) cathode electrode with active material; (c) anode current collector, (d) cathode current collector.

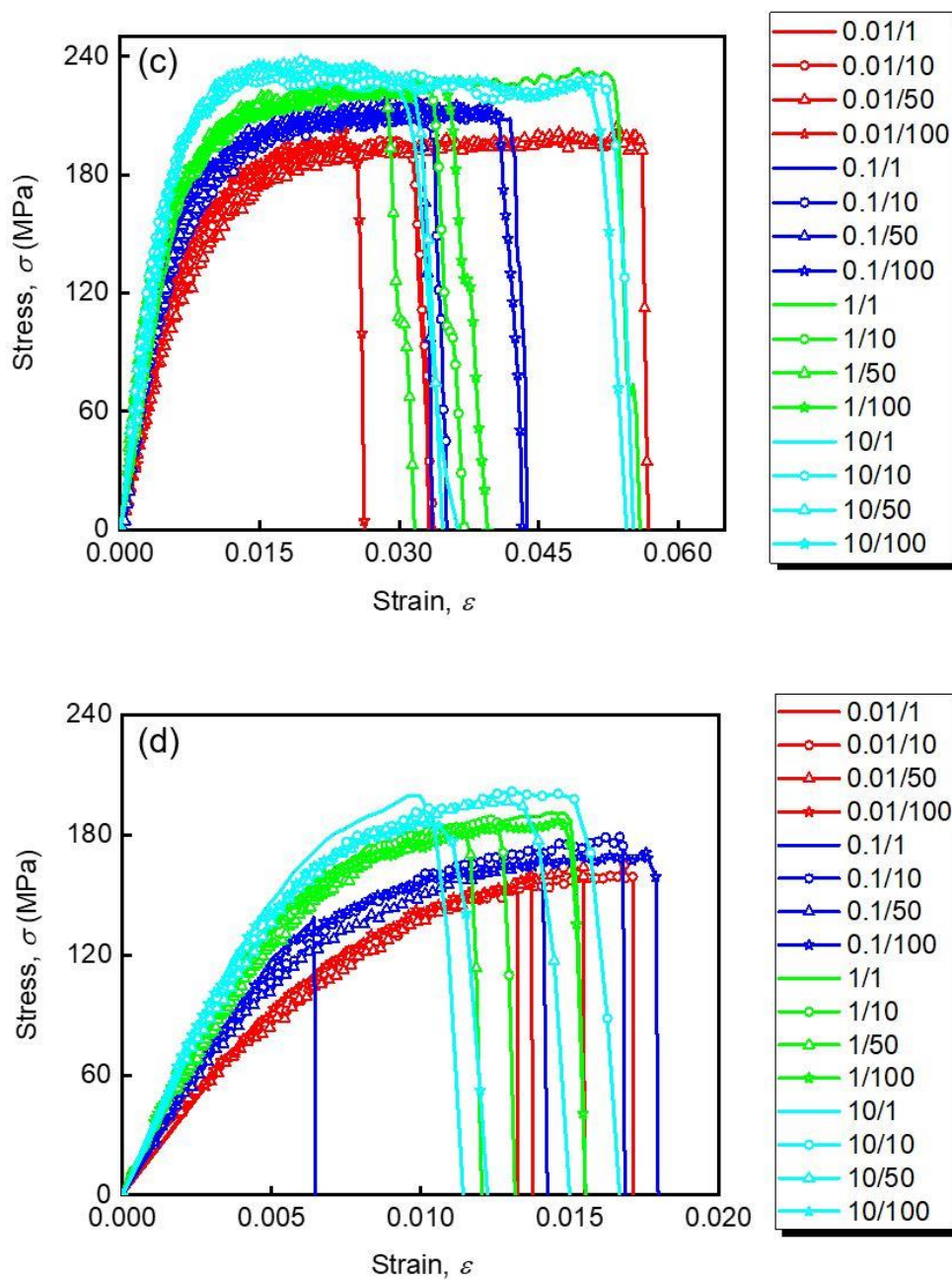


Figure 36: Stress vs strain curve comparing number of cycles at 1-C, SOC=0, 0° for (a) anode electrode with active material, (b) cathode electrode with active material; (c) anode current collector, (d) cathode current collector. (continued)

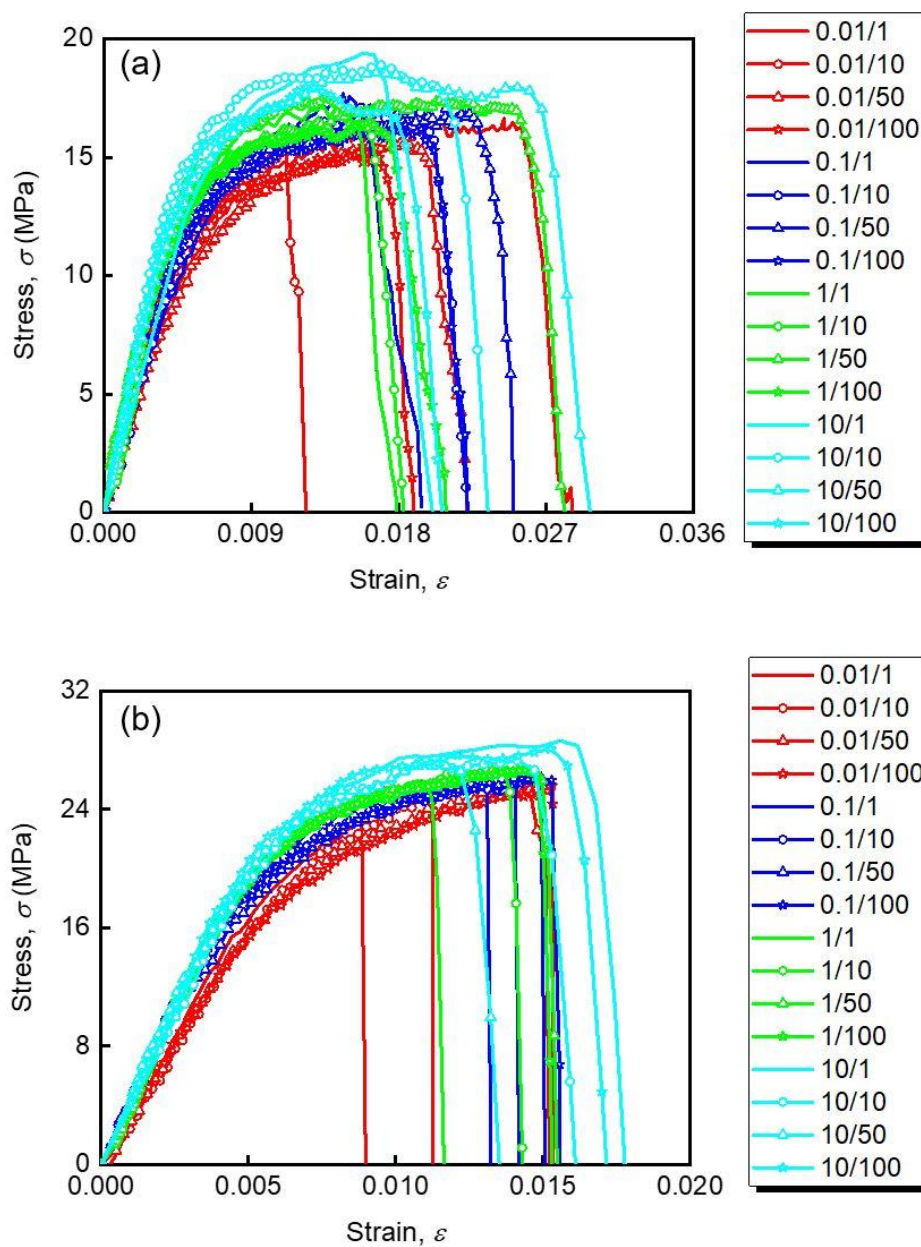


Figure 37: Stress vs strain curve comparing number of cycles at 2-C, SOC=0, 0° for (a) anode electrode with active material, (b) cathode electrode with active material; (c) anode current collector, (d) cathode current collector.

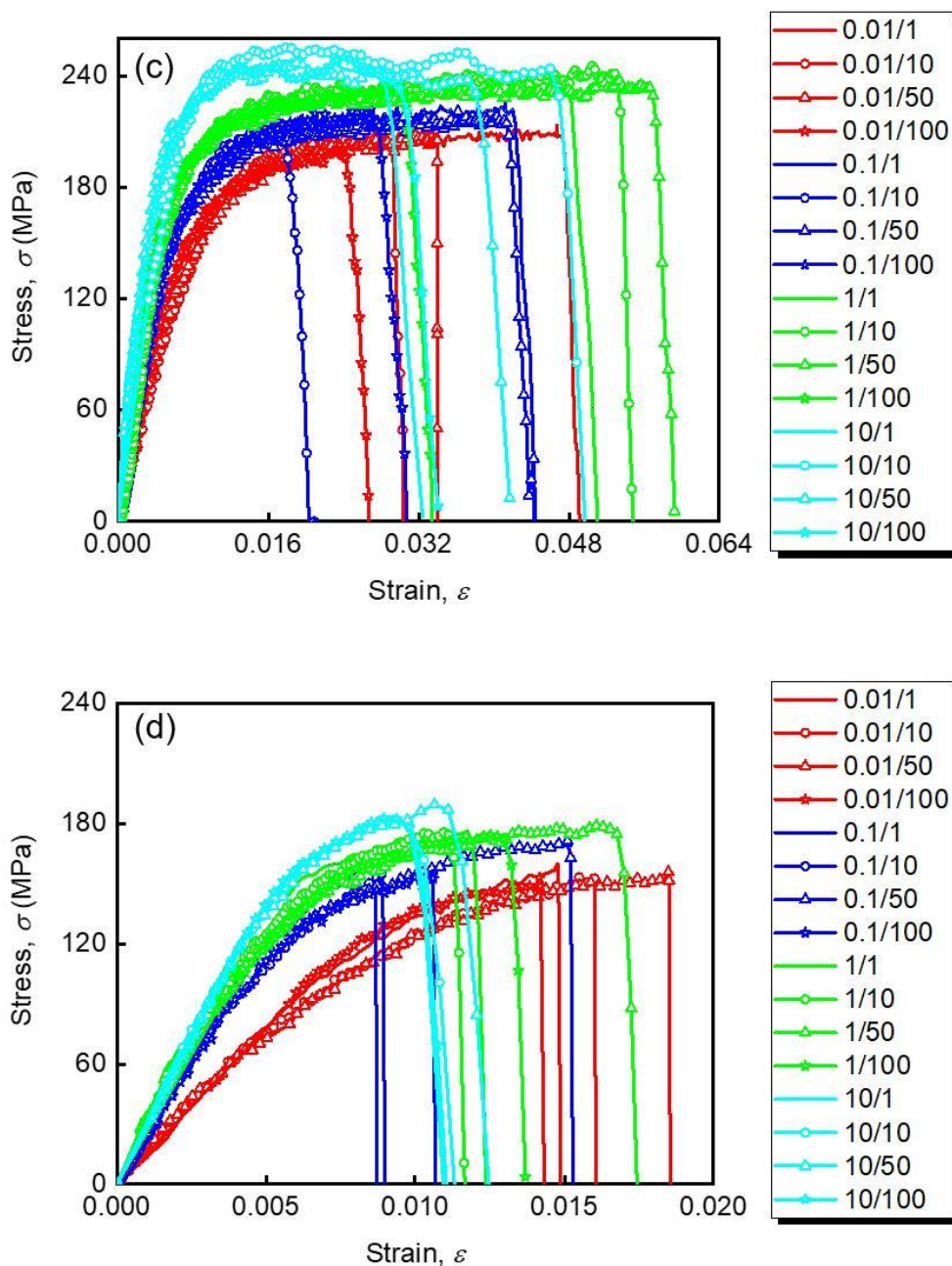


Figure 37: Stress vs strain curve comparing number of cycles at 2-C, SOC=0, 0° for (a) anode electrode with active material, (b) cathode electrode with active material; (c) anode current collector, (d) cathode current collector. (continued)

4.6. Interfacial binder effect

A comparable huge strength is noticeable in the stress-strain curves of electrodes and current collector samples. The major reason for the variation in stress is due to the thickness of the electrode with active material being larger than the thickness of the current collector. The force-displacement curve reveals the effect of the binder on the active material and current collector. The manufacturing adhesion and cohesion properties of the binder significantly influence the strength of electrodes. Chen et al. studied the interfacial binder effect on the Si/C composite anodes revealing the electrochemical reactivity of the binder materials with cycling performances and capacity retention with advanced binders [84]. This binder phenomenon also promotes the mechanical integrity behavior of the lithium-ion batteries [62, 67, 85]. Figure 38 shows provide proof of the claim. The electrode samples with active material sustain a larger load before failure than the current collector samples. This phenomenon is similar in both electrodes. Binder adhesion strength in electrodes is responsible for a 0.1 kN to 1 kN increase in the overall strength of the electrodes. However, the failure displacements and hence the failure strains of the electrode with active material are lower than the current collector for anode electrode. However, for cathode electrode, these failure displacements are not related to the binder properties.

The cathode electrode samples have nearly the same curves at lower loading velocity from 0.01/s to 1/s but at the higher velocity viz. 10/s the interfacial binder effect observed. Contrasting to the cathode, anode electrode samples show distinctive force-displacement curves at all the loading speeds.

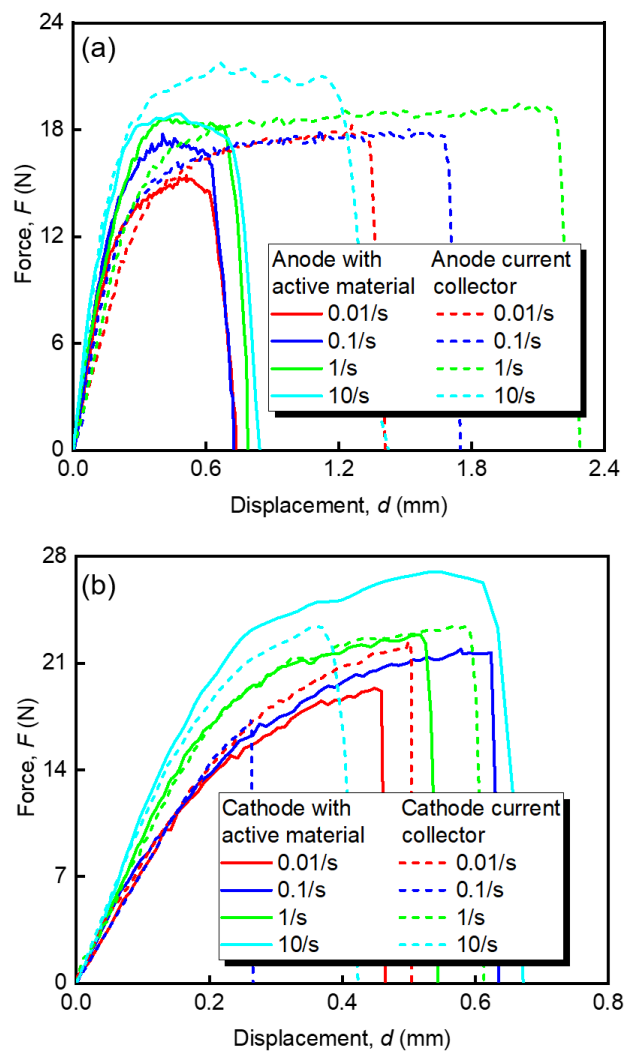


Figure 38: Force vs displacement curves at 1 cycle, 1-C charging rate, SOC=0 comparing (a) anode electrode with active material and anode current collector, (b) cathode electrode with active material and cathode current collector.

Table 5: Summary of increase/decrease in strength of electrode samples with active material and current collector with various phenomenon

Phenomenon ▼	Sample ▶	Anode electrode with active material			Cathode electrode with active material			Anode current collector	Cathode current collector	
Orientation		0°	45°	90°	0°	45°	90°	0°	45°	90°
Strain rate effect ↑		0.01 < 0.1 < 1 < 10			0.01 < 0.1 < 1 < 10			0.01 < 0.1 < 1 < 10	0.01 < 0.1 < 1 < 10	
Anisotropic/isotropic behavior		Anisotropic			Anisotropic			Isotropic	Isotropic	
SOC effect (increasing SOC) An - ↑, Ca - ↓		0 < 0.2 < 0.4 < 0.6			0.6 < 0.4 < 0.2 < 0			No effect	0.6 < 0.4 < 0.2 < 0	
Charging rate effect		1-C ≥ 0.5-C > 0.1-C > 2-C			No effect			No effect	No effect	
Cycling effect ↓ (increasing number of cycles)		100 < 50 < 10 < 1			100 < 50 < 10 < 1			No effect	No effect	

CHAPTER 5: CONCLUSION

21700 is a recent addition to the commercial battery. Due to the high-density and power density of this battery, the mechanical behavior study is a trending topic of discussion. A fundamental understanding of the 18650 LIBs mechanical loading and the behavior study of the electrochemical status of the battery, electrodes have provided an ample perception to execute this thesis study.

This study has performed an elaborate experimental testing and numerical simulation work, considering each parameter that can be varied to deeply understand the mechanical behavior of these 21700 M50 LIB cells. The parameters investigated were the strain rates 0.01/s, 0.1/s, 1/s, and 10/s; SOC 0, 0.2, 0.4, and 0.6; anisotropic behavior study for orientation of battery samples in 0°, 45° and 90°; charging rates of 0.1-C, 0.5-C, 1-C and 2-C; charging/discharging cycle of 1, 10, 50 and 100.

Based on the numerical simulation validation for the conducted experiments results extracted following conclusions were drawn and are listed as follows:

- The mechanical and electrochemical properties show an excellent agreement with the anisotropic behavior for the electrodes (i.e., anode and cathode), and the current collectors show isotropic behavior at the mentioned three orientations.
- All the samples of the electrode and current collectors for investigated with variable parameters combination have proved to be highly strain rate dependent.
- Anode, cathode, and cathode current collectors have a significant SOC effect influence the mechanical behavior of the said samples. The anode current collector has indicated no change due to SOC. With the increase of SOC from

0 to 0.6 the anode electrode has increment in comparable curves, whereas the cathode and its current collector have shown a decrement in comparable curves.

- The cathode electrode, anode current collector, and cathode current collector are independent of the charging rates mannered. Anode electrode has reasoned with the charging rates with a multivariant run for charge/discharge cycle from 1 to 100.
- The cycling does not have a noticeable impact on the mechanical behavior of the anode and cathode current collectors. For the anode electrode with the cycle increment, electrodes weaken and hence degrade the performance. The similar tendency is observed for cathode electrodes at lower charging rates of 0.1-C and 0.5-C, but at 1-C and 2-C, the cathode shows behavior independent of the cycling rate.
- The interfacial effect from the binder in between the active materials and the current collectors is more discernible in anode than in cathode. This effect contributes to the mechanical and electrochemical integrity of 21700 lithium-ion batteries.

The behavior of electrodes with active material and the respective current collector at the various effects investigated is summarized in Table 5.

A comprehensive characterization supplementing mechanical and electrochemical behavior of electrodes and respective current collectors of 21700 M50 lithium-ion batteries and useful numerical models has favored the future safety design, evaluation, and monitoring of the batteries.

REFERENCES

- [1] S. Abada, G. Marlair, A. Lecocq, M. Petit, V. Sauvant-Moynot and F. Huet. Safety focused modeling of lithium-ion batteries: A review, *Journal of Power Sources* 306 (2016) 178-192.
- [2] B. Scrosati and J. Garche. Lithium batteries: Status, prospects and future, *Journal of Power Sources* 195 (2010) 2419-2430.
- [3] G. Kermani and E. Sahraei. Review: Characterization and Modeling of the Mechanical Properties of Lithium-Ion Batteries, *Energies* 10 (2017)
- [4] M. A. Hannan, M. S. H. Lipu, A. Hussain and A. Mohamed. A review of lithium-ion battery state of charge estimation and management system in electric vehicle applications: Challenges and recommendations, *Renewable and Sustainable Energy Reviews* 78 (2017) 834-854.
- [5] B. Liu, Y. Jia, C. Yuan, L. Wang, X. Gao, S. Yin and J. Xu. Safety issues and mechanisms of lithium-ion battery cell upon mechanical abusive loading: A review, *Energy Storage Materials* 24 (2020) 85-112.
- [6] L. Hollmotz. Safety of lithium ion batteries in vehicles: state of the art, risks and trends, *Proceedings of the 23 rd International Technical Conference on the Enhanced Safety of Vehicles*, Seoul, South Korea (2013)
- [7] G. E. Blomgren. The Development and Future of Lithium Ion Batteries, *Journal of The Electrochemical Society* 164 (2016) A5019-A5025.
- [8] B. Liu, Y. Jia, J. Li, S. Yin, C. Yuan, Z. Hu, L. Wang, Y. Li and J. Xu. Safety issues caused by internal short circuits in lithium-ion batteries, *Journal of Materials Chemistry A* 6 (2018) 21475-21484.

- [9] V. Etacheri, R. Marom, R. Elazari, G. Salitra and D. Aurbach. Challenges in the development of advanced Li-ion batteries: a review, *Energy & Environmental Science* 4 (2011) 3243-3262.
- [10] X. Zhang, P. N. Ross, R. Kostecki, F. Kong, S. Sloop, J. B. Kerr, K. Striebel, E. J. Cairns and F. McLarnon. Diagnostic Characterization of High Power Lithium-Ion Batteries for Use in Hybrid Electric Vehicles, *Journal of The Electrochemical Society* 148 (2001)
- [11] J. B. Goodenough and Y. Kim. Challenges for Rechargeable Li Batteries†, *Chemistry of Materials* 22 (2010) 587-603.
- [12] D. Lisbona and T. Snee. A review of hazards associated with primary lithium and lithium-ion batteries, *Process Safety and Environmental Protection* 89 (2011) 434-442.
- [13] E. Sahraei, M. Kahn, J. Meier and T. Wierzbicki. Modelling of cracks developed in lithium-ion cells under mechanical loading, *RSC Advances* 5 (2015) 80369-80380.
- [14] E. Sahraei, J. Campbell and T. Wierzbicki. Modeling and short circuit detection of 18650 Li-ion cells under mechanical abuse conditions, *Journal of Power Sources* 220 (2012) 360-372.
- [15] E. Sahraei, J. Meier and T. Wierzbicki. Characterizing and modeling mechanical properties and onset of short circuit for three types of lithium-ion pouch cells, *Journal of Power Sources* 247 (2014) 503-516.
- [16] X. Zhang, W. Shyy and A. Marie Sastry. Numerical Simulation of Intercalation-Induced Stress in Li-Ion Battery Electrode Particles, *Journal of The Electrochemical Society* 154 (2007)
- [17] D. Shi, X. Xiao, X. Huang and H. Kia. Modeling stresses in the separator of a pouch lithium-ion cell, *Journal of Power Sources* 196 (2011) 8129-8139.

- [18] K. Smith, G.-H. Kim, E. Darcy and A. Pesaran. Thermal/electrical modeling for abuse-tolerant design of lithium ion modules, *International Journal of Energy Research* 34 (2010) 204-215.
- [19] P. Barai, K. Smith, C.-F. Chen, G.-H. Kim and P. P. Mukherjee. Reduced Order Modeling of Mechanical Degradation Induced Performance Decay in Lithium-Ion Battery Porous Electrodes, *Journal of The Electrochemical Society* 162 (2015) A1751-A1771.
- [20] J. Xu, B. Liu, X. Wang and D. Hu. Computational model of 18650 lithium-ion battery with coupled strain rate and SOC dependencies, *Applied Energy* 172 (2016) 180-189.
- [21] J. Xu, L. Wang, J. Guan and S. Yin. Coupled effect of strain rate and solvent on dynamic mechanical behaviors of separators in lithium ion batteries, *Materials & Design* 95 (2016) 319-328.
- [22] K. Zhao, M. Pharr, J. J. Vlassak and Z. Suo. Fracture of electrodes in lithium-ion batteries caused by fast charging, *Journal of Applied Physics* 108 (2010)
- [23] B. Wu and W. Lu. A battery model that fully couples mechanics and electrochemistry at both particle and electrode levels by incorporation of particle interaction, *Journal of Power Sources* 360 (2017) 360-372.
- [24] J. Xu, B. Liu and D. Hu. State of Charge Dependent Mechanical Integrity Behavior of 18650 Lithium-ion Batteries, *Sci Rep* 6 (2016) 21829.
- [25] J. Xu, Y. Jia, B. Liu, H. Zhao, H. Yu, J. Li and S. Yin. Coupling Effect of State-of-Health and State-of-Charge on the Mechanical Integrity of Lithium-Ion Batteries, *Experimental Mechanics* 58 (2018) 633-643.

- [26] L. Wang, S. Yin, C. Zhang, Y. Huan and J. Xu. Mechanical characterization and modeling for anodes and cathodes in lithium-ion batteries, *Journal of Power Sources* 392 (2018) 265-273.
- [27] H. Maleki and J. N. Howard. Internal short circuit in Li-ion cells, *Journal of Power Sources* 191 (2009) 568-574.
- [28] P. Peng and F. Jiang. Thermal safety of lithium-ion batteries with various cathode materials: A numerical study, *International Journal of Heat and Mass Transfer* 103 (2016) 1008-1016.
- [29] P. Ping, Q. Wang, P. Huang, J. Sun and C. Chen. Thermal behaviour analysis of lithium-ion battery at elevated temperature using deconvolution method, *Applied Energy* 129 (2014) 261-273.
- [30] E. Sahraei, E. Bosco, B. Dixon and B. Lai. Microscale failure mechanisms leading to internal short circuit in Li-ion batteries under complex loading scenarios, *Journal of Power Sources* 319 (2016) 56-65.
- [31] C. Yuan, X. Gao, H. K. Wong, B. Feng and J. Xu. A Multiphysics Computational Framework for Cylindrical Battery Behavior upon Mechanical Loading Based on LS-DYNA, *Journal of The Electrochemical Society* 166 (2019) A1160-A1169.
- [32] L. Greve and C. Fehrenbach. Mechanical testing and macro-mechanical finite element simulation of the deformation, fracture, and short circuit initiation of cylindrical Lithium ion battery cells, *Journal of Power Sources* 214 (2012) 377-385.
- [33] R. M. Spotnitz, J. Weaver, G. Yeduvaka, D. Doughty and E. Roth. Simulation of abuse tolerance of lithium-ion battery packs, *Journal of power sources* 163 (2007) 1080-1086.
- [34] T. Kisters, E. Sahraei and T. Wierzbicki. Dynamic impact tests on lithium-ion cells, *International Journal of Impact Engineering* 108 (2017) 205-216.

- [35] I. Avdeev and M. Gilaki. Structural analysis and experimental characterization of cylindrical lithium-ion battery cells subject to lateral impact, *Journal of Power Sources* 271 (2014) 382-391.
- [36] W. Cai, H. Wang, H. Maleki, J. Howard and E. Lara-Curzio. Experimental simulation of internal short circuit in Li-ion and Li-ion-polymer cells, *Journal of Power Sources* 196 (2011) 7779-7783.
- [37] J. Lamb and C. J. Orendorff. Evaluation of mechanical abuse techniques in lithium ion batteries, *Journal of Power Sources* 247 (2014) 189-196.
- [38] M. Raffler, A. Sevarin, C. Ellersdorfer, S. F. Heindl, C. Breiffuss and W. Sinz. Finite element model approach of a cylindrical lithium ion battery cell with a focus on minimization of the computational effort and short circuit prediction, *Journal of Power Sources* 360 (2017) 605-617.
- [39] C. Zhang, S. Santhanagopalan, M. A. Sprague and A. A. Pesaran. Coupled mechanical-electrical-thermal modeling for short-circuit prediction in a lithium-ion cell under mechanical abuse, *Journal of Power Sources* 290 (2015) 102-113.
- [40] C. Zhang, S. Santhanagopalan, M. A. Sprague and A. A. Pesaran. A representative-sandwich model for simultaneously coupled mechanical-electrical-thermal simulation of a lithium-ion cell under quasi-static indentation tests, *Journal of Power Sources* 298 (2015) 309-321.
- [41] X. Zhang, E. Sahraei and K. Wang. Deformation and failure characteristics of four types of lithium-ion battery separators, *Journal of Power Sources* 327 (2016) 693-701.
- [42] X. Zhang and T. Wierzbicki. Characterization of plasticity and fracture of shell casing of lithium-ion cylindrical battery, *Journal of Power Sources* 280 (2015) 47-56.
- [43] M. Gilaki and I. Avdeev. Impact modeling of cylindrical lithium-ion battery cells: a heterogeneous approach, *Journal of Power Sources* 328 (2016) 443-451.

- [44] B. Liu, J. Zhang, C. Zhang and J. Xu. Mechanical integrity of 18650 lithium-ion battery module: Packing density and packing mode, *Engineering Failure Analysis* 91 (2018) 315-326.
- [45] M. Khan, M. Swierczynski and S. Kær. Towards an Ultimate Battery Thermal Management System: A Review, *Batteries* 3 (2017)
- [46] Y. Chen, S. Santhanagopalan, V. Babu and Y. Ding. Dynamic mechanical behavior of lithium-ion pouch cells subjected to high-velocity impact, *Composite Structures* 218 (2019) 50-59.
- [47] T. Wierzbicki and E. Sahraei. Homogenized mechanical properties for the jellyroll of cylindrical Lithium-ion cells, *Journal of Power Sources* 241 (2013) 467-476.
- [48] M. Y. Ali, W.-J. Lai and J. Pan. Computational models for simulation of a lithium-ion battery module specimen under punch indentation, *Journal of Power Sources* 273 (2015) 448-459.
- [49] V. Ruiz, A. Pfrang, A. Kriston, N. Omar, P. Van den Bossche and L. Boon-Brett. A review of international abuse testing standards and regulations for lithium ion batteries in electric and hybrid electric vehicles, *Renewable and Sustainable Energy Reviews* 81 (2018) 1427-1452.
- [50] J. Zhu, X. Zhang, E. Sahraei and T. Wierzbicki. Deformation and failure mechanisms of 18650 battery cells under axial compression, *Journal of Power Sources* 336 (2016) 332-340.
- [51] B. Liu, S. Yin and J. Xu. Integrated computation model of lithium-ion battery subject to nail penetration, *Applied Energy* 183 (2016) 278-289.
- [52] W.-J. Lai, M. Y. Ali and J. Pan. Mechanical behavior of representative volume elements of lithium-ion battery modules under various loading conditions, *Journal of Power Sources* 248 (2014) 789-808.

- [53] W.-J. Lai, M. Y. Ali and J. Pan. Mechanical behavior of representative volume elements of lithium-ion battery cells under compressive loading conditions, *Journal of Power Sources* 245 (2014) 609-623.
- [54] A. A. Franco. Multiscale modelling and numerical simulation of rechargeable lithium ion batteries: concepts, methods and challenges, *RSC Advances* 3 (2013)
- [55] E. Sahraei, R. Hill and T. Wierzbicki. Calibration and finite element simulation of pouch lithium-ion batteries for mechanical integrity, *Journal of Power Sources* 201 (2012) 307-321.
- [56] D. Grazioli, M. Magri and A. Salvadori. Computational modeling of Li-ion batteries, *Computational Mechanics* 58 (2016) 889-909.
- [57] J. Kukreja, T. Nguyen, T. Siegmund, W. Chen, W. Tsutsui, K. Balakrishnan, H. Liao and N. Parab. Crash analysis of a conceptual electric vehicle with a damage tolerant battery pack, *Extreme Mechanics Letters* 9 (2016) 371-378.
- [58] L. Lu, X. Han, J. Li, J. Hua and M. Ouyang. A review on the key issues for lithium-ion battery management in electric vehicles, *Journal of Power Sources* 226 (2013) 272-288.
- [59] A. Barré, B. Deguilhem, S. Grolleau, M. Gérard, F. Suard and D. Riu. A review on lithium-ion battery ageing mechanisms and estimations for automotive applications, *Journal of Power Sources* 241 (2013) 680-689.
- [60] A. W. Golubkov, D. Fuchs, J. Wagner, H. Wiltsche, C. Stangl, G. Fauler, G. Voitic, A. Thaler and V. Hacker. Thermal-runaway experiments on consumer Li-ion batteries with metal-oxide and olivin-type cathodes, *Rsc Advances* 4 (2014) 3633-3642.
- [61] R. Marom, S. F. Amalraj, N. Leifer, D. Jacob and D. Aurbach. A review of advanced and practical lithium battery materials, *Journal of Materials Chemistry* 21 (2011) 9938-9954.

- [62] L. Wang, X. Duan, B. Liu, Q. M. Li, S. Yin and J. Xu. Deformation and failure behaviors of anode in lithium-ion batteries: Model and mechanism, *Journal of Power Sources* 448 (2020)
- [63] X. Gao, P. He, J. Ren and J. Xu. Modeling of contact stress among compound particles in high energy lithium-ion battery, *Energy Storage Materials* 18 (2019) 23-33.
- [64] S. S. Zhang. A review on the separators of liquid electrolyte Li-ion batteries, *Journal of Power Sources* 164 (2007) 351-364.
- [65] Q. Wang, J. Sun, X. Yao and C. Chen. Thermal Behavior of Lithiated Graphite with Electrolyte in Lithium-Ion Batteries, *Journal of The Electrochemical Society* 153 (2006)
- [66] P. Zuo and Y.-P. Zhao. A phase field model coupling lithium diffusion and stress evolution with crack propagation and application in lithium ion batteries, *Physical Chemistry Chemical Physics* 17 (2015) 287-297.
- [67] H. Luo, J. Zhu, E. Sahraei and Y. Xia. Adhesion strength of the cathode in lithium-ion batteries under combined tension/shear loadings, *RSC advances* 8 (2018) 3996-4005.
- [68] S. Zhang, M. Sakane, T. Nagasawa and K. Kobayashi. Mechanical Properties of Copper Thin Films Used in Electronic Devices, *Procedia Engineering* 10 (2011) 1497-1502.
- [69] X. Jiang, H. Luo, Y. Xia and Q. Zhou. Mechanical Behavior of Lithium-Ion Battery Component Materials and Error Sources Analysis for Test Results, *SAE International Journal of Materials and Manufacturing* 9 (2016) 614-621.
- [70] Z. Pan, T. Sedlatschek and Y. Xia. Effect of State-of-Charge and Air Exposure on Tensile Mechanical Properties of Lithium-Ion Battery Electrodes, *Journal of The Electrochemical Society* 167 (2020)

- [71] C. Yuan, L. Wang, S. Yin and J. Xu. Generalized separator failure criteria for internal short circuit of lithium-ion battery, *Journal of Power Sources* 467 (2020)
- [72] P. M. Gomadam, J. W. Weidner, R. A. Dougal and R. E. White. Mathematical modeling of lithium-ion and nickel battery systems, *Journal of power sources* 110 (2002) 267-284.
- [73] G. G. Botte, V. R. Subramanian and R. E. White. Mathematical modeling of secondary lithium batteries, *Electrochimica Acta* 45 (2000) 2595-2609.
- [74] B. Y. Liaw, R. G. Jungst, G. Nagasubramanian, H. L. Case and D. H. Doughty. Modeling capacity fade in lithium-ion cells, *Journal of Power Sources* 140 (2005) 157-161.
- [75] M. Safari, M. Morcrette, A. Teyssot and C. Delacourt. Life prediction methods for lithium-ion batteries derived from a fatigue approach: Ii. capacity-loss prediction of batteries subjected to complex current profiles, *Journal of The Electrochemical Society* 157 (2010) A892.
- [76] J. Shim, R. Kosteki, T. Richardson, X. Song and K. A. Striebel. Electrochemical analysis for cycle performance and capacity fading of a lithium-ion battery cycled at elevated temperature, *Journal of power sources* 112 (2002) 222-230.
- [77] J. Wen, Y. Yu and C. Chen. A Review on Lithium-Ion Batteries Safety Issues: Existing Problems and Possible Solutions, *Materials Express* 2 (2012) 197-212.
- [78] S. Santhanagopalan, Q. Guo, P. Ramadass and R. E. White. Review of models for predicting the cycling performance of lithium ion batteries, *Journal of Power Sources* 156 (2006) 620-628.
- [79] W. Fang, P. Ramadass and Z. Zhang. Study of internal short in a Li-ion cell-II. Numerical investigation using a 3D electrochemical-thermal model, *Journal of Power Sources* 248 (2014) 1090-1098.

- [80] W. Mei, L. Zhang, J. Sun and Q. Wang. Experimental and numerical methods to investigate the overcharge caused lithium plating for lithium ion battery, *Energy Storage Materials* 32 (2020) 91-104.
- [81] L. Wang, S. Yin and J. Xu. A detailed computational model for cylindrical lithium-ion batteries under mechanical loading: From cell deformation to short-circuit onset, *Journal of Power Sources* 413 (2019) 284-292.
- [82] J. Zhu, J. Feng and Z. Guo. Mechanical properties of commercial copper current-collector foils, *RSC Adv.* 4 (2014) 57671-57678.
- [83] E. Kramer, S. Passerini and M. Winter. Dependency of Aluminum Collector Corrosion in Lithium Ion Batteries on the Electrolyte Solvent, *ECS Electrochemistry Letters* 1 (2012) C9-C11.
- [84] L. Chen, X. Xie, J. Xie, K. Wang and J. Yang. Binder effect on cycling performance of silicon/carbon composite anodes for lithium ion batteries, *Journal of Applied Electrochemistry* 36 (2006) 1099-1104.
- [85] J. Chen, J. Liu, Y. Qi, T. Sun and X. Li. Unveiling the Roles of Binder in the Mechanical Integrity of Electrodes for Lithium-Ion Batteries, *Journal of The Electrochemical Society* 160 (2013) A1502-A1509.